This document was prepared in conjunction with work accomplished under Contract No. DE-AC09-96SR18500 with the U. S. Department of Energy.

DISCLAIMER

X-ray Computed Tomography and Stereo-Radiographic Inspection Results of the Office of Emergency Response (NA-42) Test Object

---

Final Report
WSRC-TR-2005-00472

October 2005

Submitted by:

Kenneth M. Gibbs, PhD
Joel D. Jones

Savannah River National Laboratory

Table of Contents

Introduction

The purpose of this report is to document the results of work funded by the Office of Emergency Response (NA-42) to investigate methods for noninvasive inspection of improvised nuclear devices. The ultimate goal of the inspection methods is to obtain targeting information so that such a device may be disabled and rendered inert. This targeting information should be obtained in the shortest period of time possible, due to the serious consequences associated with a failure to deactivate the device.

The team at Savannah River National Laboratory performed an initial cursory x-ray radiographic examination of the object using photostimulable luminescent phosphor plates (an alternative to film), performed computed tomography (CT) with a custom built digital radiography system, investigated the effects of limited view data on the fidelity of the CT reconstruction, and also demonstrated the effectiveness of a two-view stereo-radiographic technique using both object rotation and source translation methodologies. The stereo-radiographic results were validated using the CT results.

Description of the Test Object

The NA-42 Test Object is a nondescript plywood crate which contains a simulated improvised nuclear device (IND). The exterior dimensions of the crate were 48 inches long, 36 inches tall, and 32 inches wide. The diagonal distance across the top, which represents the largest dimension to be imaged, was about 58 inches. The enlargement factor (or magnification) due to the x-ray fan angle of the x-ray radiographic inspection system for the center of the crate was approximately (141/104 or 1.36). Thus, the 58 inch dimension would be enlarged to about 79 inches. Consequently, a custom large image format (85” wide) digital radiography system was assembled using existing equipment to support the CT inspection.

Initial Survey of Test Object

After receiving the NA-42 Test Object in early June 2005, an initial survey inspection was performed using photostimulable luminscent (PSL) phosphor screens. The PSL plates are 14 x 17 inches and a number of the plates were used simultaneously to produce mosaic images. Images at 0 and 90 degrees are shown in Figures 1 and 2. The use of PSL screens eliminates the need for film and the associated chemical processing, but offers comparable resolution (80 micron). The screens are loaded in light-tight cassettes similar to film. The screens are generally more sensitive than film and require shorter exposures. For this application, the exposure time was 7 seconds for 300kV, 2.1 mA, at 120 inches.

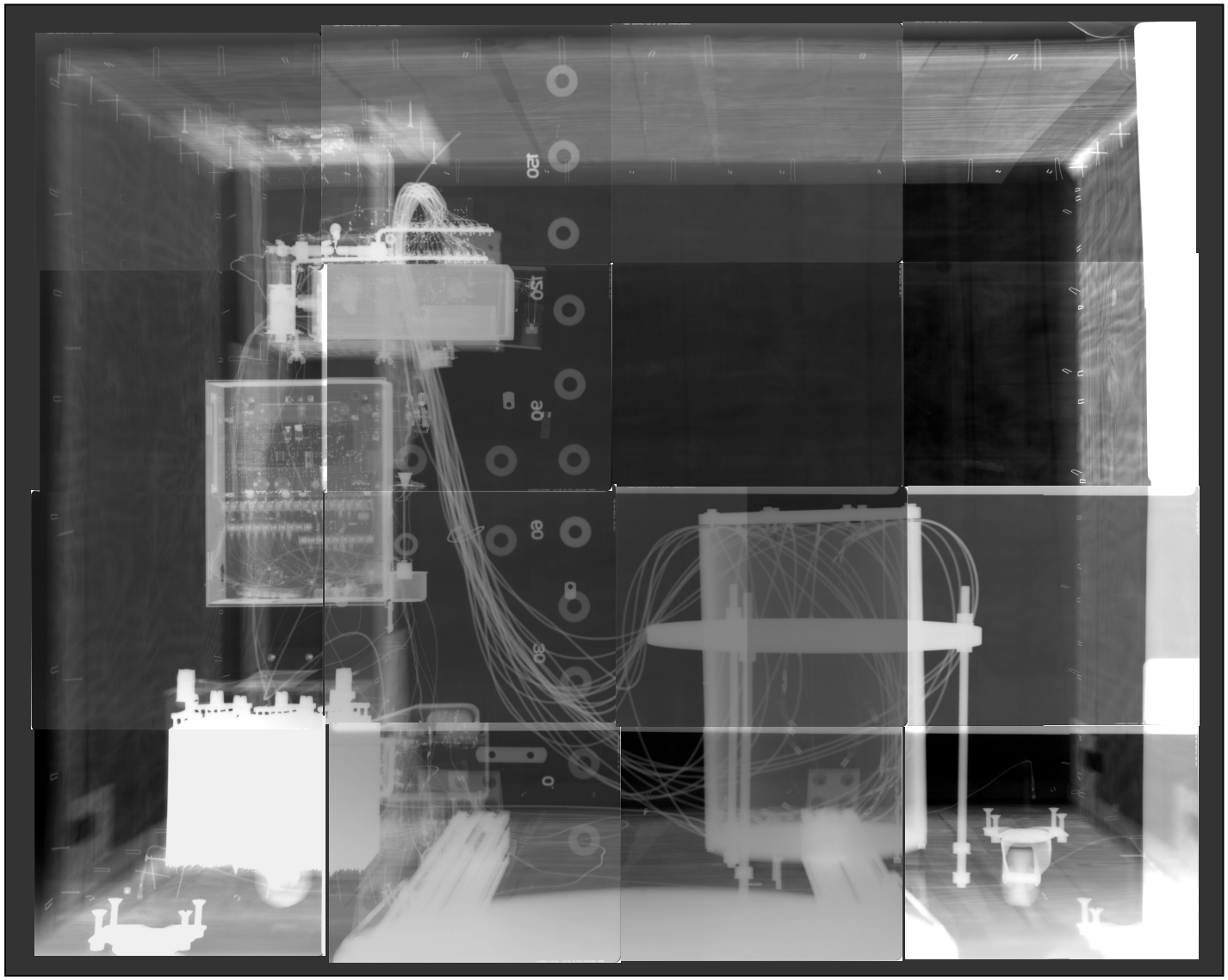

Figure 1: High resolution, mosaic image of test object in the 0 degree orientation produced using PSL plates.

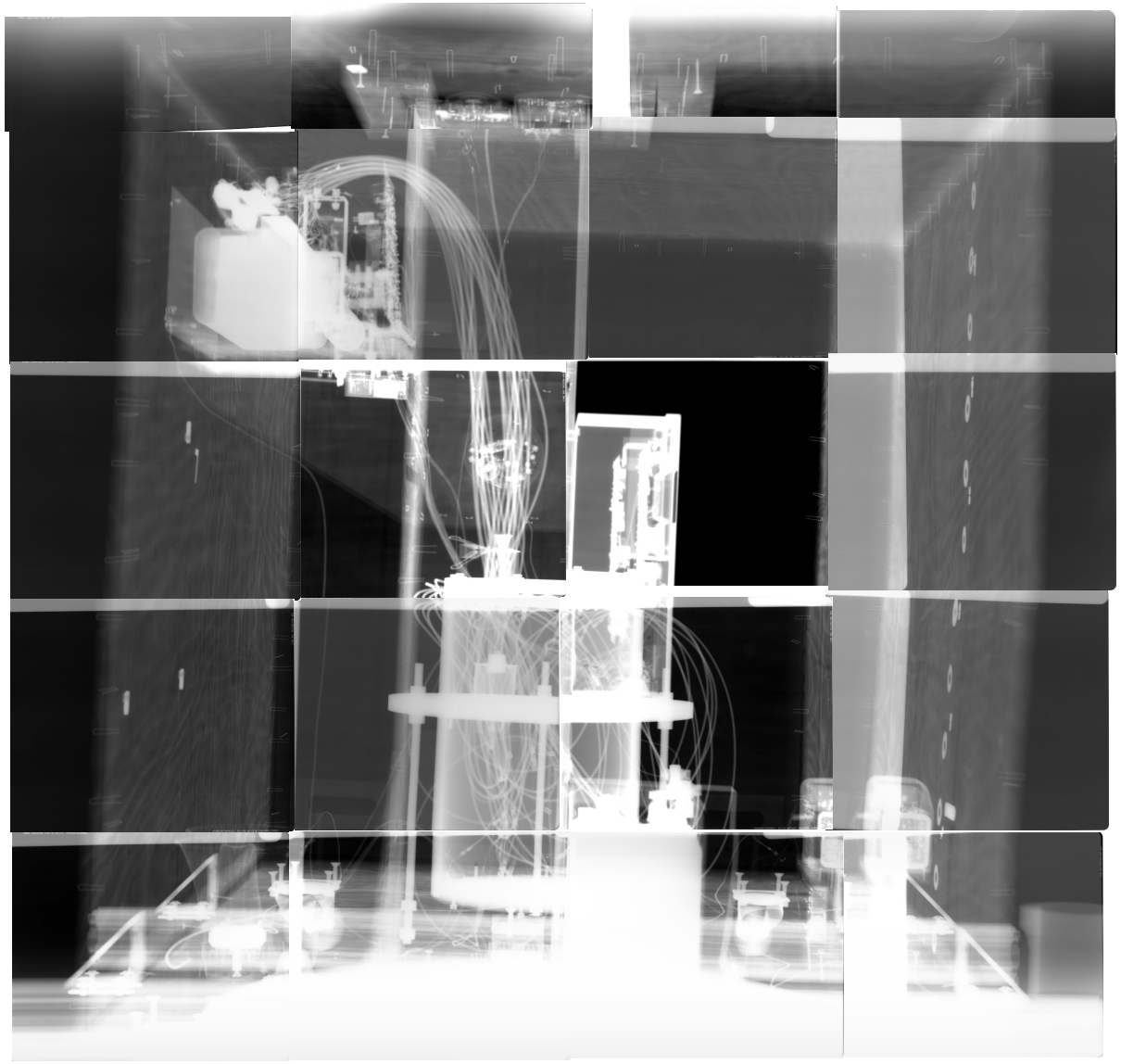

Figure 2: High resolution, mosaic image of test object in the 90 degree orientation produced using PSL plate.

Following exposure, the screens are laser scanned to produce a digital image. Figure 3 shows a set of cassettes and the laser scanner from one manufacturer. The size of our scanner is about the size of two laserjet printers. The need for a laser scanner and computer is the only disadvantage of this technology for field use. However, manufacturers have been making progress in reducing the size of the scanners.

Another alternative for large format (14 x 17 inch), low profile, digital x-ray imaging is the amorphous silicon (ASi) flat panel imager shown in Figure 4. This system produces a digital x-ray directly. Thus, a field system would consist of the low profile imager, power supply, and a laptop computer.

Both the PSL and ASi options could be used in much the same way as film is currently used, especially in situations where the IND may have limited access. For example, if a suspect device is located in a corner of a building or shipping container, these detectors can be used with 1/2 inch of clearance, whereas other systems (such as portable CT systems) would not be practical. This topic will be discussed further later in the report.

Figure 3: PSL cassettes and laser scanner.

Figure 4: Amorphous silicon flat panel imager.

Computed Tomography Results

A custom CT system with a 17 x 85 inch field-of-view (FOV) was constructed for the explicit purpose of performing computed tomography on the NA-42 Test Object, which will be referred to subsequently as the "crate." The CT system consisted of a 320 kV x-ray source, rotation stage and support structure, and imaging system. The CT system is shown in Figure 5.

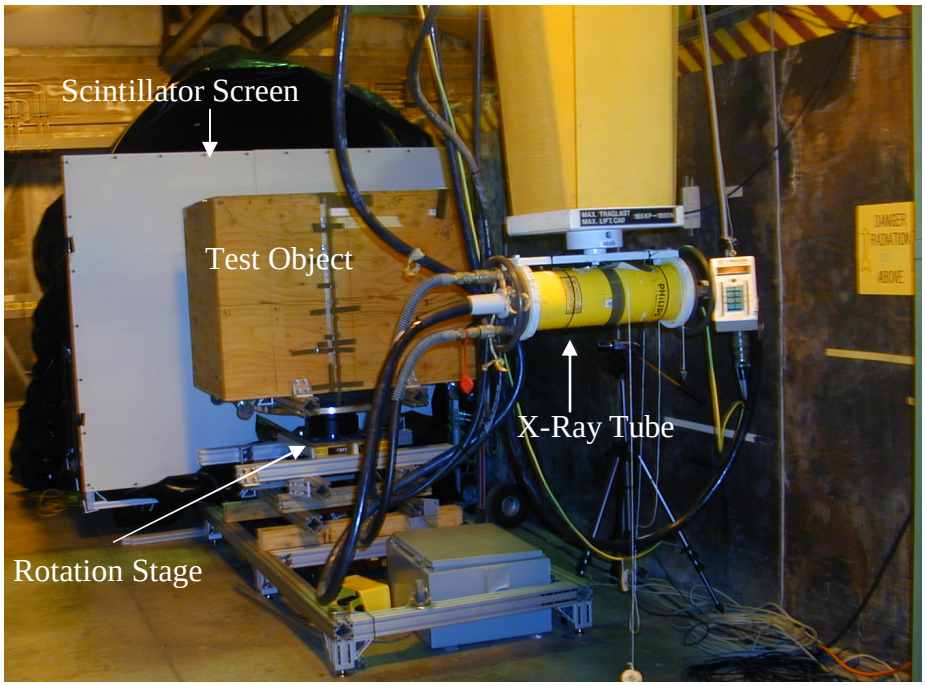

Figure 5: CT system built to image the NA-42 test object.

The imaging system consisted of a phosphor screen array, turning mirror, lens, and charge coupled device (CCD) camera. This system was enclosed in a light-tight "tent." The scintillator screen was a mosaic consisting of a 1 x 5 array of 17 x 17 inch phosphor screens. A 5 x 5 screen array could have been used, but as will be seen below, the vertical viewing height was restricted due to restrictions on the CT reconstruction software. The scintillators were gadolinium oxysulfide compound and were manufactured by MCI Optonix. The camera was a Photometrics Quantix with a 3048 x 2048 pixel scientific grade, thermo-electrically cooled CCD chip. The camera was shielded from direct exposure to the x-ray beam by lead shielding as shown in Figure 6.

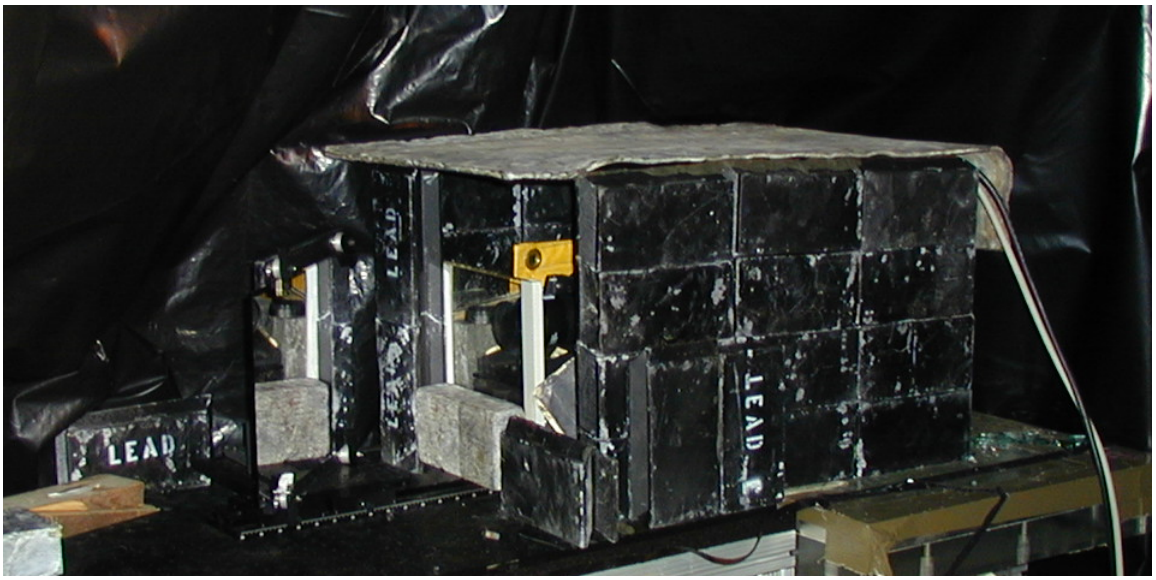

Figure 6: Imaging system with turning mirror, lens , and CCD encased in lead shielding.

The crate was imaged using x-rays at a peak energy of 300 kV and a beam current of 2.1 mA using the 1.2 x 1.2 mm focal spot. The source-to-detector distance was 141 inches and the source-to-center of rotation distance was 103 inches. Object rotation was provided by a servo-controlled rotary stage with a 30 inch diameter table. The accuracy of the table and associated control software was set to approximately 0.05 degrees. Due to the size of the crate, a secondary support structure was attached to the table, to support and secure the crate during imaging.

Tomographic reconstruction was performed using the Feldcamp algorithm for cone beam geometry. A caveat with this algorithm is that for cone angles greater than about 5 degrees the geometric distortion in the reconstruction, caused by the use of tilted fans as an approximation for conic projections, becomes significant. With a cone angle of about 16 degrees, it was decided to perform the CT in four vertical segments to limit the cone angle in each section to a maximum of about 3 degrees. The source was vertically centered in the FOV for each segment, which involved moving the source vertically.

Prior to performing CT, external markers were placed on the crate to provide known reference markings. The markers were 1.25 inch steel washers spaced at approximately 3 inches apart from the top to the bottom of the crate on the side facing the source at the 0 degree orientation. There were 12 washers in all and steel bars were placed at the fourth, seventh, and tenth spacers. The purpose of the steel bars was to facilitate merging the images from the 4 segments. In addition, T-handle allen wrenches were placed at the top center of the front and rear faces. The shafts acted as the sights of a rifle and were used to align the center-of-rotation of the stage with the center of the scintillator array, and the x-ray beam centerline.

Given the equipment and experimental setup described above, Table 1 shows the trade-offs between sensor binning, reconstructed image resolution, exposure time, number of projections, data collection (scan) time, and required reconstruction time. Sensor binning refers to the lumping together or integrating the charge collected on the sensor. A 1 x 1 bin indicates that

there is no binning and each pixel value is retained. Conversely, an 8 x 8 bin sums the charge of 64 pixels in an 8 x 8 array. Binning reduces the exposure time by the square of the bin factor but degrades the spatial resolution by the bin factor. It was determined that the required exposure time for a 1 x 1 bin was 160 seconds per images and the resolution was 0.0275 inches. At a 8 x 8 bin the exposure time per image was reduced by a factor of 64 to 2.5 seconds at the expense of a degradation of the resolution to 0.22 inches.

Table 1: CT data collection and reconstruction parameters.

Sensor Binning	N. Rays	Recon. Res. (inch)	Exp. Time (sec)	Move Time (sec)	Proj. Time (sec)	N Proj.	Vert. Scans	Rows/ Scan	Total Scan Time (hr)	Recon Time (hr)
8 x 8	381	0.22	2.5	5	7.5	360	4	62	3.0	0.17
4 x 4	762	0.11	10	5	15	720	4	124	12.0	1.50
2 x 2	1524	0.055	40	5	45	1524	4	248	76.2	13.92
1 x 1	3048	0.0275	160	5	165	3048	4	496	558.8	122.40

The number of rays is the width of the sensor in pixels divided by the bin factor. The move time is the time required to move to the next view angle. This time was treated as a constant value but actually would increase somewhat with increasing number of projections because the tolerance of the servo position would become tighter due to the smaller angular interval.

Later in the report, we will investigate the affect of limiting the number of projections (limited view tomography). For now, we used the rule of thumb that the number of projections should be on the same order as the number of rays. For the 8 x 8 and 4 x 4 bin case we used angular intervals of 1 and 0.5 degrees, which resulted in 360 and 720 projections, respectively.

The projection time is the sum of the exposure time and the move time. The number of vertical scans was set to be four to limit geometric distortion due to the Feldcamp algorithm. The rows per scan value is driven by the number of vertical scans and the bin factor. The total scan time is the (projection time) x (number of projections) x (number of vertical scans). The reconstruction times were determined empirically and would be highly dependent on the particular computer on which the reconstructions were performed and could be dramatically improved with parallel processing. They are intended here mainly as a relative indication of how the reconstruction time is affected by the CT parameter selection.

Ultimately, we selected a 4 x 4 bin as a trade-off between total scan time and resolution (see the shaded row in Table 1 for all parameters). Based on the selected 4 x 4 bin, the total scan time of the object was 12 hours and the time to perform the reconstructions was about 1.5 hours. These times were considered reasonable and the lower bin factors had unacceptably high data collection times (76 and 559 hours).

At the beginning of the program, SRNL was informed (via telecom with Tom Weber) that the resolution goal for targeting was a value of 1 mm (or 0.039 inch). As can be seen in Table 1, the 1 x 1 case just exceeds the desired resolution, but a 559 hour data collection time and 122 hour reconstruction time would be not be practical in a field environment.

We conclude that it is not practical to provide a system with the desired resolution (0.039 inches) and field-of-view (85 inches) needed for this particular test object, based on a lens coupled CCD with phosphor scintillating screens. Even with screens 10 times brighter than those used, the total scan time would be on the order of 60 hours. However, this statement will be revisited in the limited view CT section. However, for a "full view" CT data set, where the number of projections is approximately equal to the number of rays, this statement is certainly true.

Selected CT projections at 45 degree intervals obtained with the selected parameters from Table 1 are shown in Figure 7. All 720 views are recorded in a "movie" (Projection.avi) file which is on the CD-ROM provided with this report. This movie can be viewed using Windows Media Player or other appropriate software. If the reader is viewing this document in Microsoft Word, the movie can be viewed by a <CTRL> <double left mouse click> on this hyperlink (Projections.avi).

The projections alone provide valuable information regarding the test object. Multiple views of the crate reveal components that may be otherwise obscured. Display in a "movie" format provides a qualitative "feel" for the contents. As will be shown below, in the section on stereo-radiography from object rotation, two or more of these projection images can be used to determine the location of selected target points within the object without the need for tomographic reconstruction.

The projections can also be used to produce slices perpendicular to the axis of rotation by using tomographic reconstruction. As mentioned above, the Feldcamp Cone Beam Reconstruction algorithm was used to produces the results in Figure 8. All slices are recorded in a "movie" (Slices.avi) file which is on the CD-ROM provided with this report. This movie can be viewed using Windows Media Player or other appropriate software. If the reader is viewing this document in Microsoft Word, the movie can be viewed by a <CTRL> <double left mouse click> on this hyperlink (slices.avi).

We attempt to identify a few major components in the crate in Figure 9. Since our expertise is in radiographic imaging and not weapon design, some components may be misidentified, but the point we are attempting to make is that we can supply the techniques that will provide the "weapons experts" at the scene with quality images and targeting information to assist in the task of rendering the device inert.

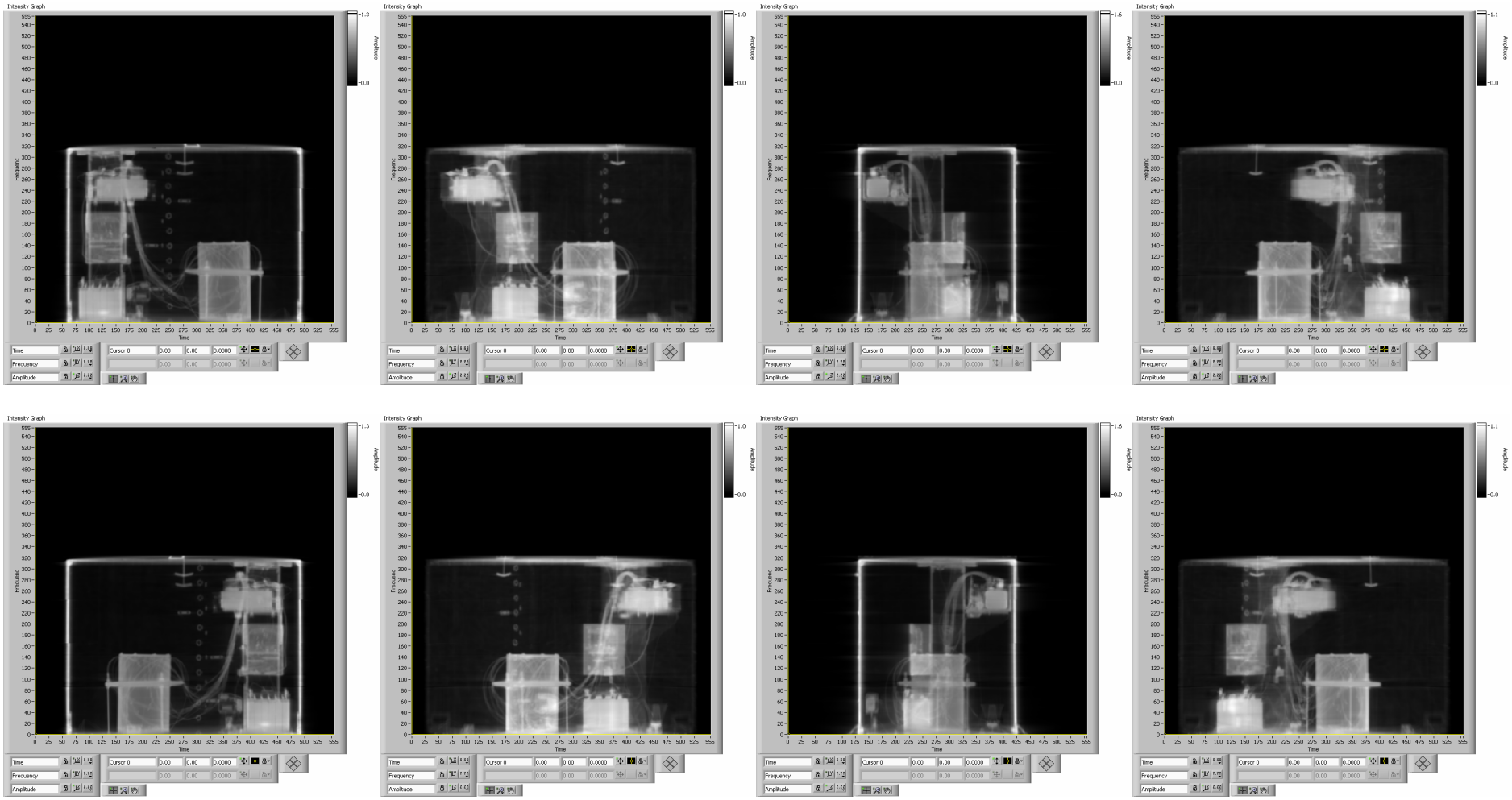

Figure 7: Static projection images at 45 degree intervals (0, 45, 90, 135, 180, 225, 270, 315 degrees from upper left) used for the CT reconstruction.

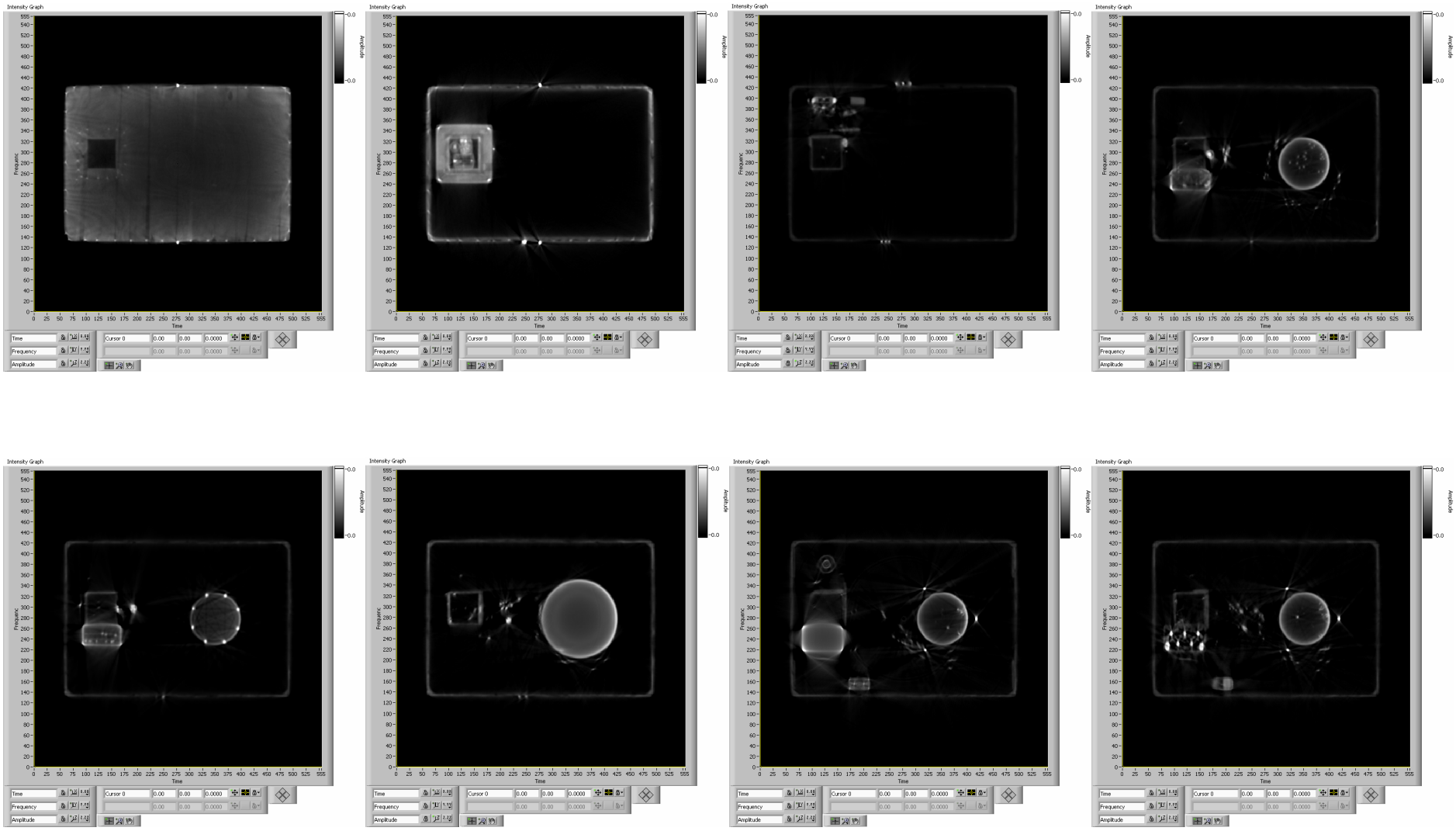

Figure 8: Selected reconstructed CT slices through the crate.

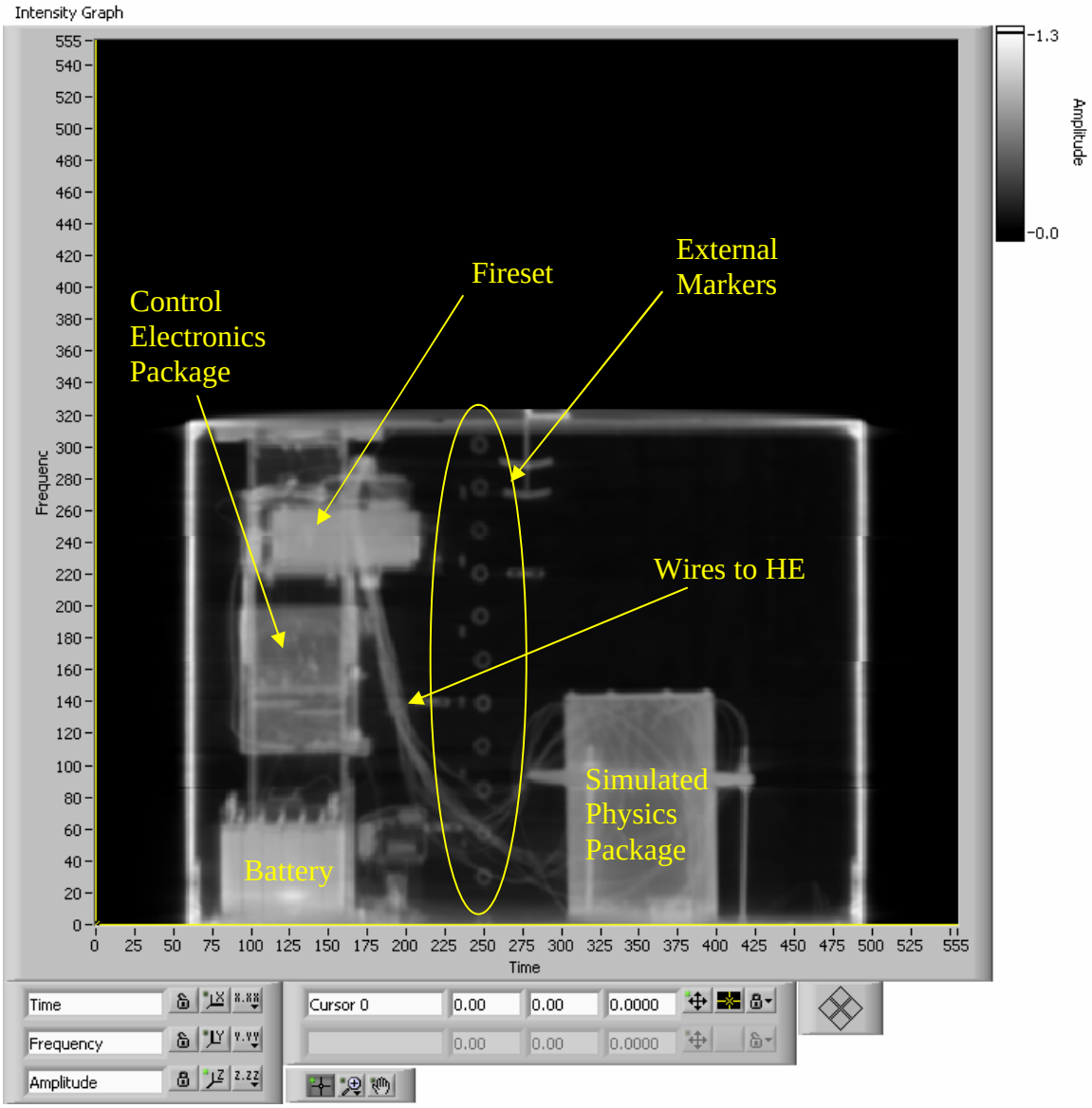

Figure 9: Identification of major device components.

Limited View CT Results

From theoretical data sampling considerations, the number of views or projections (N_{proj}) required in CT is πN_{rays}. This relationship is obtained by requiring that the angular sampling rate match the detector sampling rate (pixelization) at the edges of the reconstructed planes. However, acceptable images can be obtained with fewer projections. In fact the general rule of thumb that is often used is to set the number of projections equal to the number of rays.

In general, however, the quality of the reconstruction will be degraded by artifacts as the number of projections is decreased. The least number of required projections depends on the particular object, the region of interest in the object, the desired information, and many other factors. Hence, it is not possible to state in a global sense that the minimum number of projections is "N," where N is always the same number.

In this report, we document the affect of limited projection reconstructions on the crate in Figure 10 through Figure 17. These figures show the results for two selected planes in the crate for the various number of projections (720, 360, 180, 90, 45, 30, 20, and 10, respectively) as listed. It can be seen that the quality of the reconstruction decreases with the decreasing projections. We did not bother to go below 10 projections due to the poor quality of the reconstruction seen at 10 projections.

It should be noted that the numbers of views is highly dependent on the size and density of the desired target object. In general, it is safe to state that as the size of the desired target decreases more projections will be needed to provide adequate reconstructions. Given a target size detectability criteria, a "phantom" object could be manufactured and a better determination of the minimum number of views as a function of object size could be provided.

Lacking the target size criteria, we will assume the desired target is shown encircled in Figure 10. We will then choose the minimum number of views such that the identification and determination of the coordinates of that object is still possible. Based on these results, it appears that 20 to 30 projections provide adequate reconstructions to obtain targeting information for the selected object.

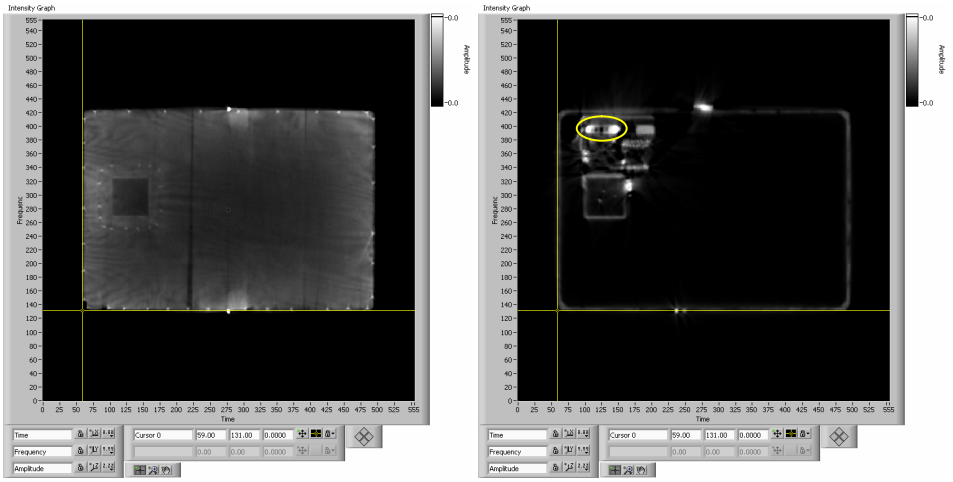

Figure 10: CT slice through the top of the crate (left) and a selected internal plane (right) for 720 projections.

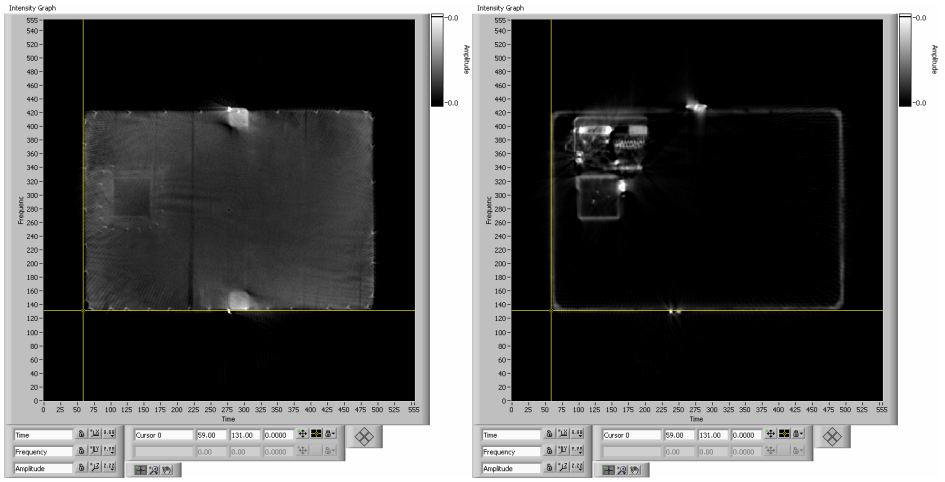

Figure 11: CT slice through the top of the crate (left) and a selected internal plane (right) for 360 projections.

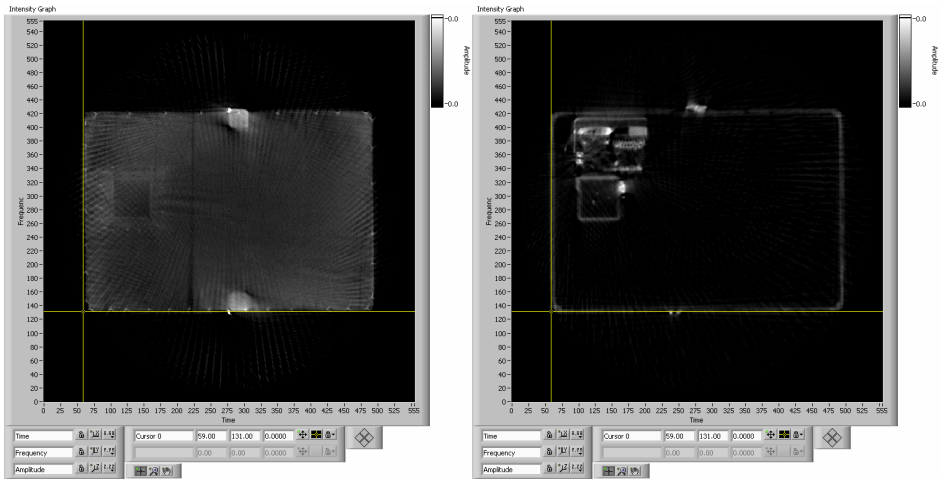

Figure 12: CT slice through the top of the crate (left) and a selected internal plane (right) for 180 projections.

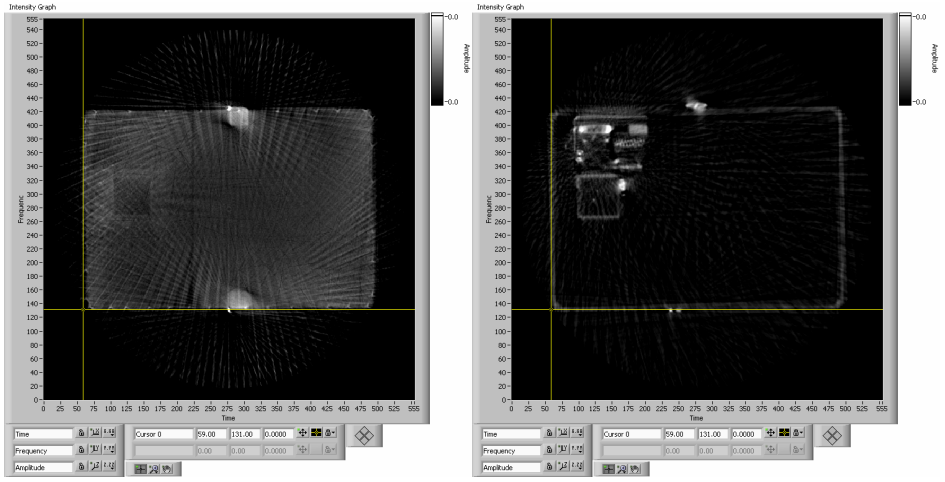

Figure 13: CT slice through the top of the crate (left) and a selected internal plane (right) for 90 projections.

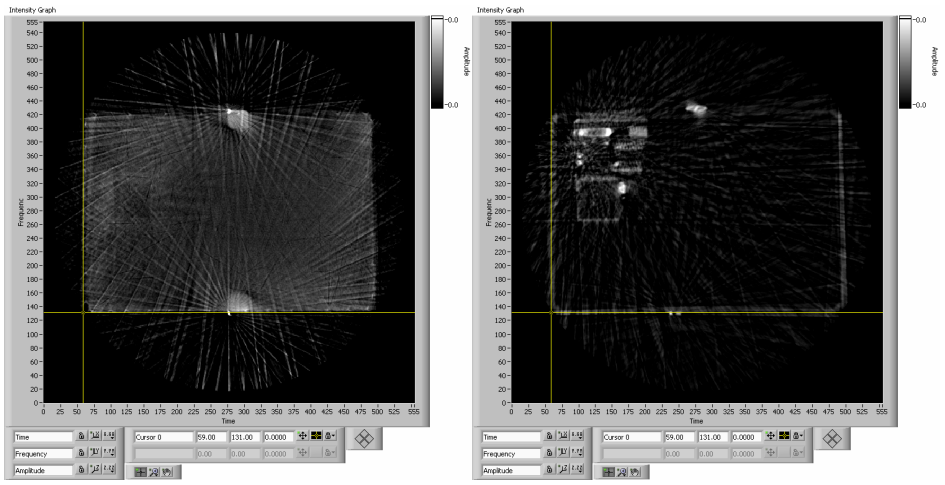

Figure 14: CT slice through the top of the crate (left) and a selected internal plane (right) for 45 projections.

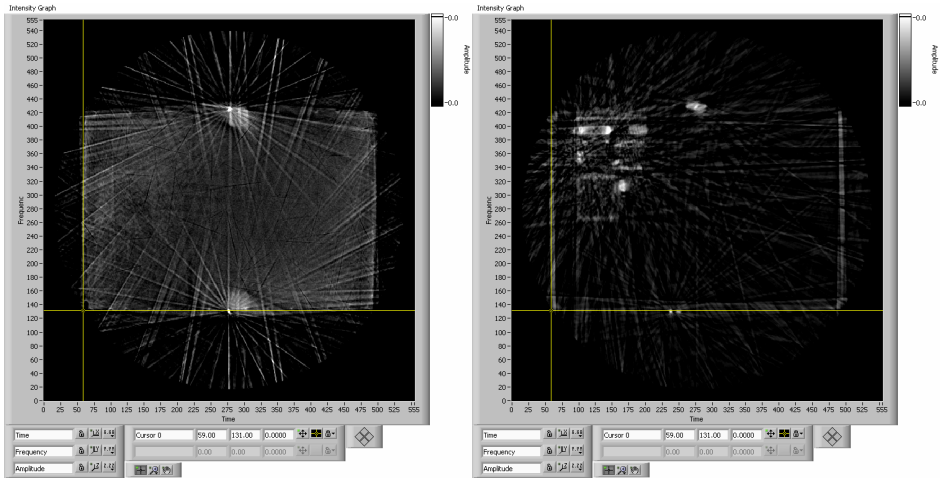

Figure 15: CT slice through the top of the crate (left) and a selected internal plane (right) for 30 projections.

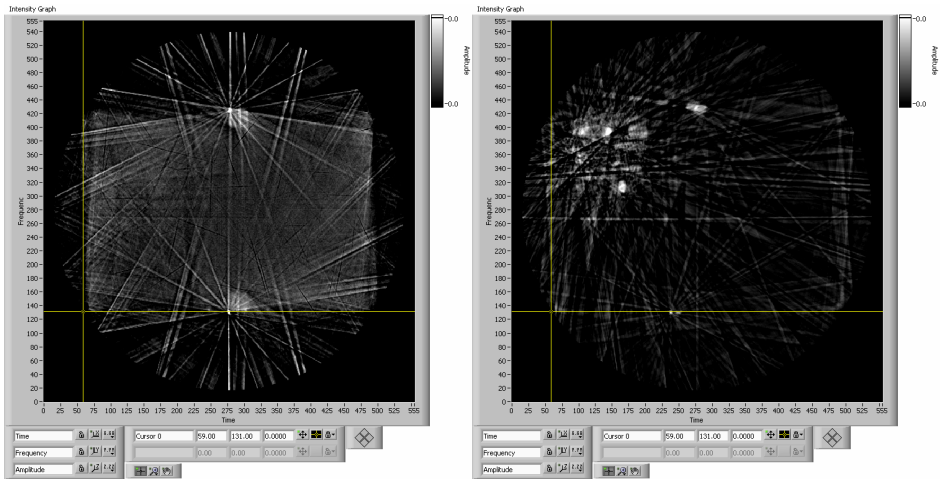

Figure 16: CT slice through the top of the crate (left) and a selected internal plane (right) for 20 projections.

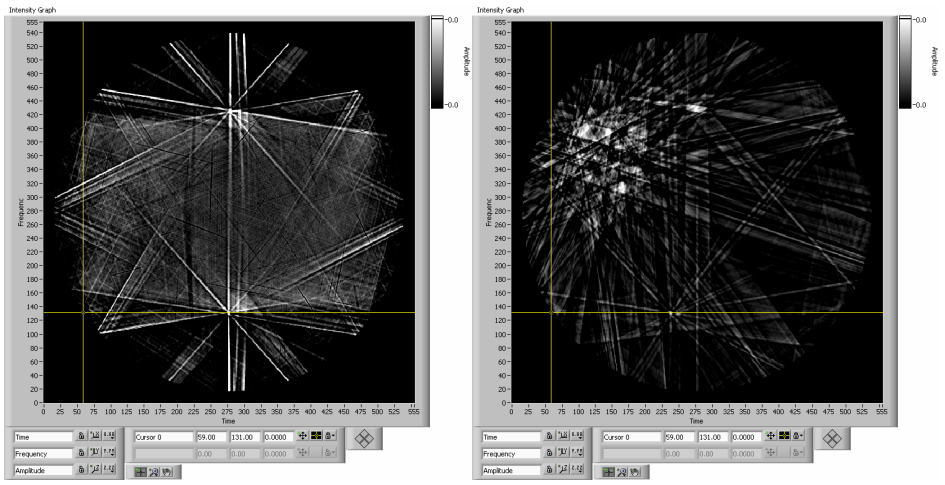

Figure 17: CT slice through the top of the crate (left) and a selected internal plane (right) for 10 projections.

To be conservative, assume that 30 projections provides the minimally acceptable image. Given this knowledge, we could then change the CT parameters to provide higher spatial resolution within an acceptable data collection time. Assuming that the ratio of the minimum number of projections to the number of rays should be about constant, this provides a method to predict the minimum number of views for higher spatial resolution setups. For example, for 720 views and a spatial resolution of 0.1094 inches, the ratio would be 30/720 or 0.0417. Thus, for 1 x 1 binning the predicted minimum number of views would be 128 (0.0417 x 3048). At a resolution of 0.0275 inches and using limited view CT, the total scan time would be reduced from 559 hours to 23.5 hours. With a more efficient scintillator or a higher flux x-ray source, this time could be substantially reduced to the point where it may be considered feasible.

Similarly, at 2 x 2 binning the predicted minimum number of views would be 64 (0.0417 x 1524). At a resolution of 0.055 inches and using limited view CT, the total scan time would be reduced from 76.2 hours to 3.2 hours. Thus, with the system described herein, it would be feasible to obtain CT data and reconstruct within 5 hours with a spatial resolution of approximately 0.055 inches. Again, with a more efficient scintillator or a higher flux x-ray source, this time could be substantially reduced even further.

Lastly, if we are willing to accept the resolution at 4 x 4 binning (0.109”), the scan time can be reduced to 0.5 hours with the current system. Table 2 summarizes the arguments above and compares the CT parameters for the 1 x 1, 2 x 2, and 4 x 4 limited view cases.

The discussion above indicated that limited view CT results with the desired resolution could be obtained within a reasonable period of time with the current system. However, in a field application, there are several pertinent conditions which affect practicality.

First, due to the nature of a suspect device, it can not be moved or touched. If the object can not be moved, then the source and detector would have to be rotated around the object on a fixed axis. In addition, the current lens coupled CCD detector system would not be appropriate for a system that would be rotated around the object. A more appropriate detector technology would be a flat panel imager or line scan array. These detectors would require scanning in one or two direction, as well as the rotation, to completely cover a large object such as the test object

inspected at SRNL. This would necessitate a fairly large and mechanically complex system with tight dimensional tolerances to allow for accurate scanning.

Secondly, one can not assume full 360 degree access. For example, if the object is in a corner of a building or shipping container, CT may not be feasible. Even a limited angle inspection would be hindered by lack of access, since the source and detector are typically 180 degrees apart.

We conclude that limited view CT is possible at the desired resolution assuming a reasonable target size (much larger than the image resolution element) and no access restrictions in the field. We believe that there is a more practical and less complicated method than CT to obtain targeting information. This method will be explored in the following two sections of the report.

Table 2: Summary of Limited View CT data collection and reconstruction parameters.

Sensor Binning	N. Rays	Recon. Res. (inch)	Exp. Time (sec)	Move Time (sec)	Proj. Time (sec)	N Proj.	Vert. Scans	Rows/ Scan	Total Scan Time (hr)	Recon Time (hr)
1 x1	3048	0.0275	160	5	165	3048	4	496	558.8	122.4
1 x1	3048	0.0275	160	5	165	128	4	496	23.5	5.1
2 x 2	1524	0.055	40	5	45	1524	4	248	76.2	13.92
2 x 2	1524	0.055	40	5	45	64	4	248	3.2	1.17
4 x 4	762	0.109	10	5	15	720	4	124	12	1.50
4 x 4	762	0.109	10	5	15	30	4	124	0.5	0.062

Stereo-radiographic Targeting Results using Object Rotation

In the real world, performing CT on an object that needs to be rapidly assessed, in a location that does not allow full access, is not practical. As mentioned above, the low resolution (0.109 inch) full view CT data collection took 12 hours. Although, we concede that higher resolution limited view CT could be performed in less time. However, the upfront setup time for the equipment and post data collection processing will add to the total response time. Lastly, the size and weight of equipment may be prohibitive to a rapid response team.

Consequently, we also considered the use of stereo-radiographic imaging as a method to provide rapid assessment and target coordinates to be used for the energetic disruption of the device. The CT data which was previously collected can be used to validate the target coordinates obtained by alternative methods in this study.

The following are examples of how the stereo-radiography using object rotation can be used to obtain coordinates of targets within an unknown object. Rotation of the source and detector is equivalent to object rotation and would be the method employed on an object that could not be moved. First, consider two views of the crate at 0 and 90 degrees as shown in Figure 18.

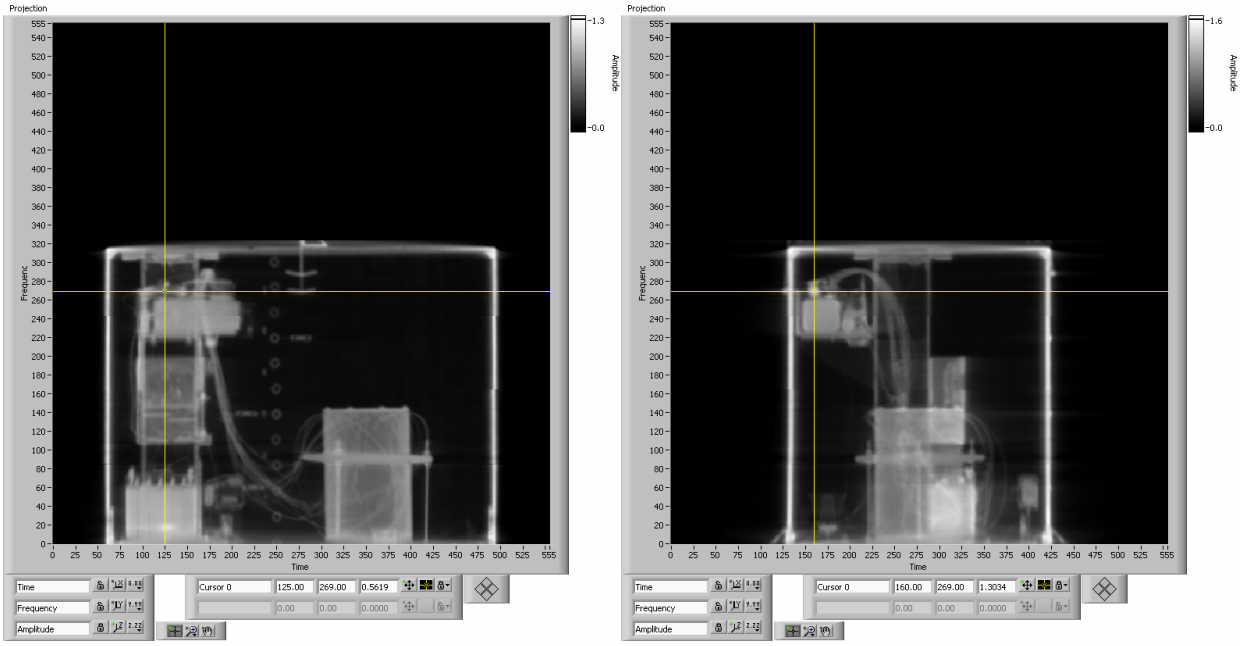

Figure 18: Two views of the object: 0 degree object rotation (left) and 90 degree object rotation (right). Note that the cursor is aligned on the same target in each view.

From the images in Figure 18, the target location, as indicated by the cursors, in the image coordinate system, (x_i,y_i), are (125,269) and (160, 269). The task is determine the coordinates of the target point with respect to a fixed reference frame on the object (x,y,z) from the image coordinates (x_i,y_i) using various transforms. The relationship between the coordinate systems used in the transforms is shown in Figure 19. The origin of the object coordinate system (x,y,z) is defined arbitrarily as the lower left front corner of the crate when looking from the source direction.

The (x',y',z') coordinate system is translated with respect to the (x, y, z) coordinate system. The origin of the (x',y',z') coordinate system is located in the center of the bottom plane of the crate, (x_0,y_0). The (x",y",z") coordinate system is rotated with respect to the (x',y',z') coordinate system by an angle θ. It is important to note that a rotation of the coordinate system by θ is equivalent to rotating the object -θ. Therefore, for the example below, θ is defined as the negative of the object rotation angle. The image coordinate system, (x_i,y_i), is related as shown. The x_i axis is parallel but translated with respect to the x" axis. The y, y', y", and y_i axes are perpendicular to the paper.

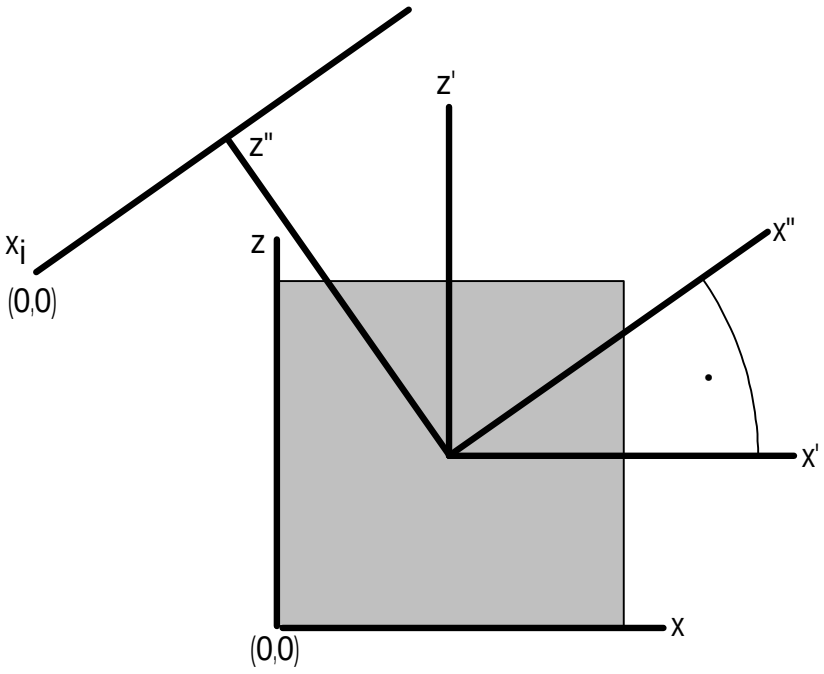

Figure 19: Relationship between coordinate systems for stereo-radiography,

Now that the relationship between the various coordinate systems has been explained, we are ready to proceed. The image coordinates of the target (x_i,y_i) are (125,269) for the 0 degree projection and (160, 269) for the 90 degree projection. The center of rotation (x_0,y_0) was determined to be (278,278). For each image, we find x" using the following relationship for both images:

$$x" = x_i - x_0$$

Thus,

$$x_1" = 125 - 278 = -153 \text{ for } \theta = -90°$$

$$x_2" = 160 - 278 = -118 \text{ for } \theta = 0°.$$

The following two equations relate the x" coordinates to the x' and z' coordinate system:

$$x_1" = x'\cos\theta_1 + z'\sin\theta_1$$

$$x_2" = x' \cos \theta_2 + z' \sin \theta_2$$

Substituting the appropriate values results in:

$$-153 = x' \cos (0) + z' \sin (0)$$
$$-118 = x' \cos (-90) + z' \sin (-90)$$

The simultaneous solution of these two equations yields:

$$x' = -153$$
$$z' = +118$$

Now, we translate back to the (x,z) coordinate system using:

$$x = x' + x_0$$
$$z = z' + z_0$$

Thus,

$$x = -153 + 278 = 125$$
$$z = +118 + 278 = 396$$

Lastly, the y coordinate is simply equal to y_i, which was 269 in both cases. Therefore, the coordinates of the target point are (125,269,396). This result can be validated by examination of the appropriate CT slice. Since the y coordinate is 269, we use slice 269 to validate the (x, z) values. As can be seen in Figure 20, the cursor is positioned in the center of the target and the cursor position is at (125,396), which correspond exactly to the (x,z) values determined above from the two projection views.

This technique seems to work well for orthogonal views, but we will now demonstrate that the technique works equally well for two arbitrary projection views. The coordinates of the target from Figure 21 are (86,268) for $\theta = -45°$ and (206,269) for $\theta = 30°$. Proceeding as in the example above, we find:

$$x_1" = 86 - 278 = -192 \text{ for } \theta = -45°$$
$$x_2" = 206 - 278 = -72 \text{ for } \theta = 30°.$$

$$-192 = x' \cos (-45) + z' \sin (-45)$$
$$-72 = x' \cos (30) + z' \sin (30)$$

$$-192 = x' (0.707) + z' (-0.707)$$
$$-72 = x' (0.866) + z' (0.5)$$

$$x' = -152.1$$
$$z' = 119.4$$

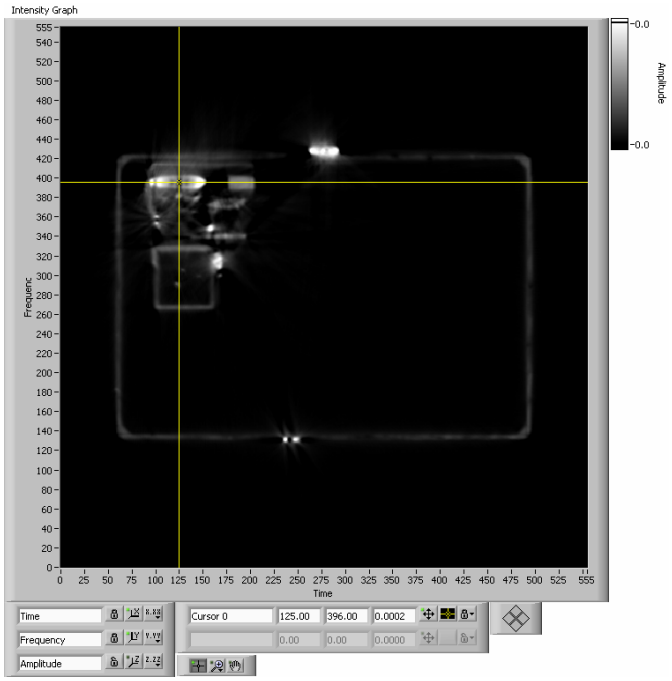

Figure 20: CT slice 269 (rCrate_1078.sdt) showing (x,z) location of target point.

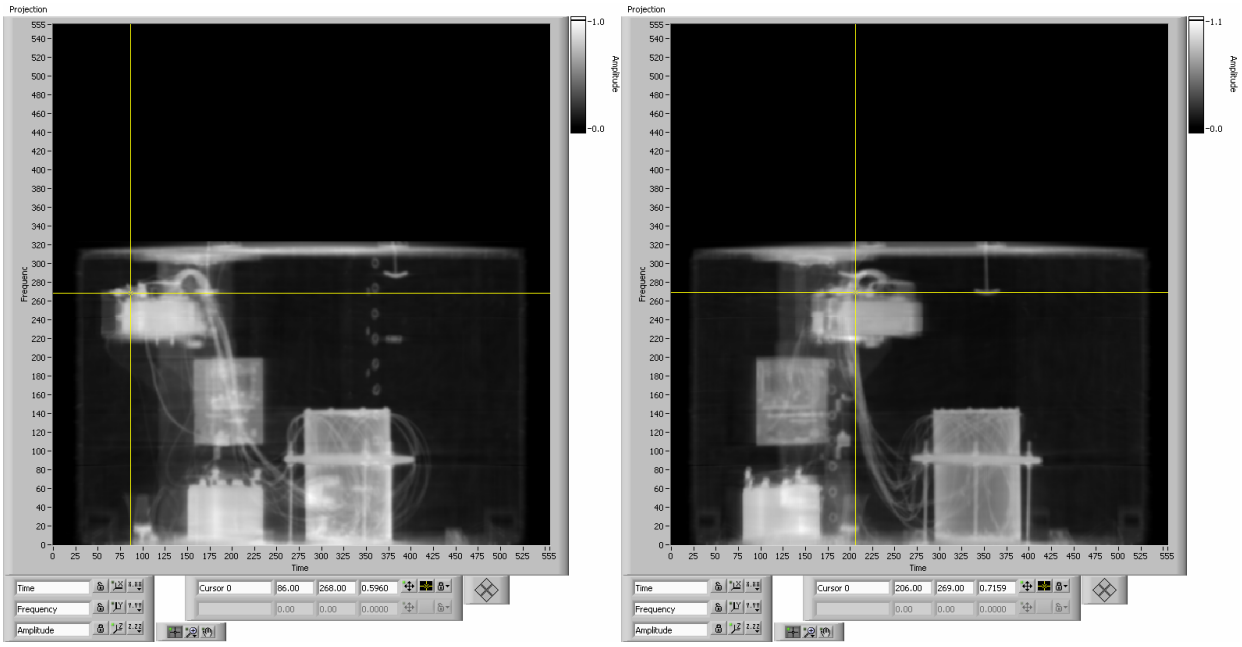

Figure 21: Two views of the object (45 degree rotation view on left and -30 degree rotation view on right) with the cursor on the same target in each view.

$$x = -152.1 + 278 = 125.9$$
$$z = 119.4 + 278 = 397.4$$

Since the y values are a little different (1 pixel off) we average those values to find 268.5. Thus, from these two views we obtain the target point of (125.9, 268.5, 397.4) as compared to (126, 269, 396). The slight error here is probably the error due to manually positioning the cursors in both views to select the same point.

At this point, a digression is in order. The coordinates have been calculated as array index values since the images have no inherent scale imbedded in the files. However, the indices can be easily converted to real world dimensions. The detector sampling size or pixel size was calculated to be 0.1498 inches. However, due to the 16.45° fan angle on the x-ray beam, the effective resolution element in the CT reconstruction space is 0.1094 inches. The pixel size can be validated by examination of the CT slice in Figure 22. Using the cursor locations indicated in the figure and the pixel size, the dimensions of the box are calculated as follows:

$$\text{Box Length} = (495\text{-}60) * (0.1094) = 47.6$$
$$\text{Box Depth} = (425\text{-}131) * (0.1094) = 32.16$$

The calculated values above agree well with the approximate dimensions of the crate, which are about 48 x 32 inches (as measured by a tape measure). The slight error is due to several factors, which include manually setting the cursor locations, the crude method (tape measure) used to obtain the crate dimensions, and the fact that the crate dimensions vary somewhat depending on where the measurement is made. Nonetheless, the result above indicates that the CT results can be considered dimensionally accurate for the purpose of validating other techniques.

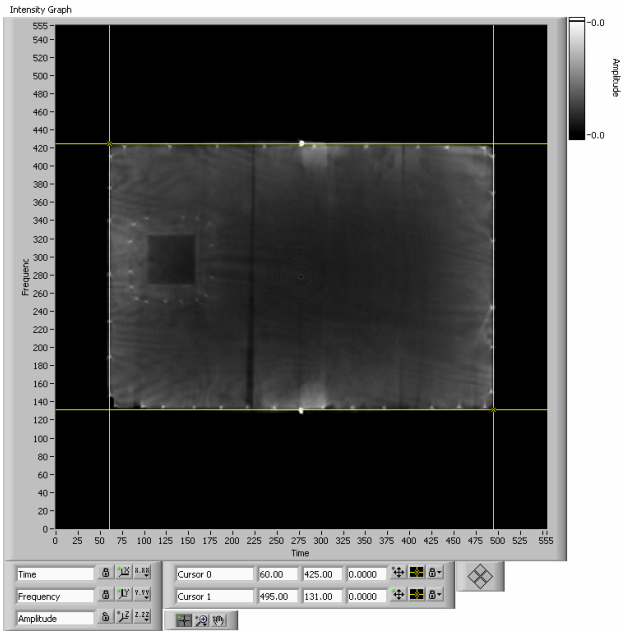

Figure 22: CT slice through the top of the crate. Note that the wood grain is visible.

As an aside, it is astounding that the wood grain of the plywood is visible in the CT reconstruction of the top.

At this point, let us consider using the stereo-radiography approach on another target point. In this mockup the wires (that in a real device would lead to the high explosives) are tightly bundled, thus we will target the wire bundle at its narrowest point.

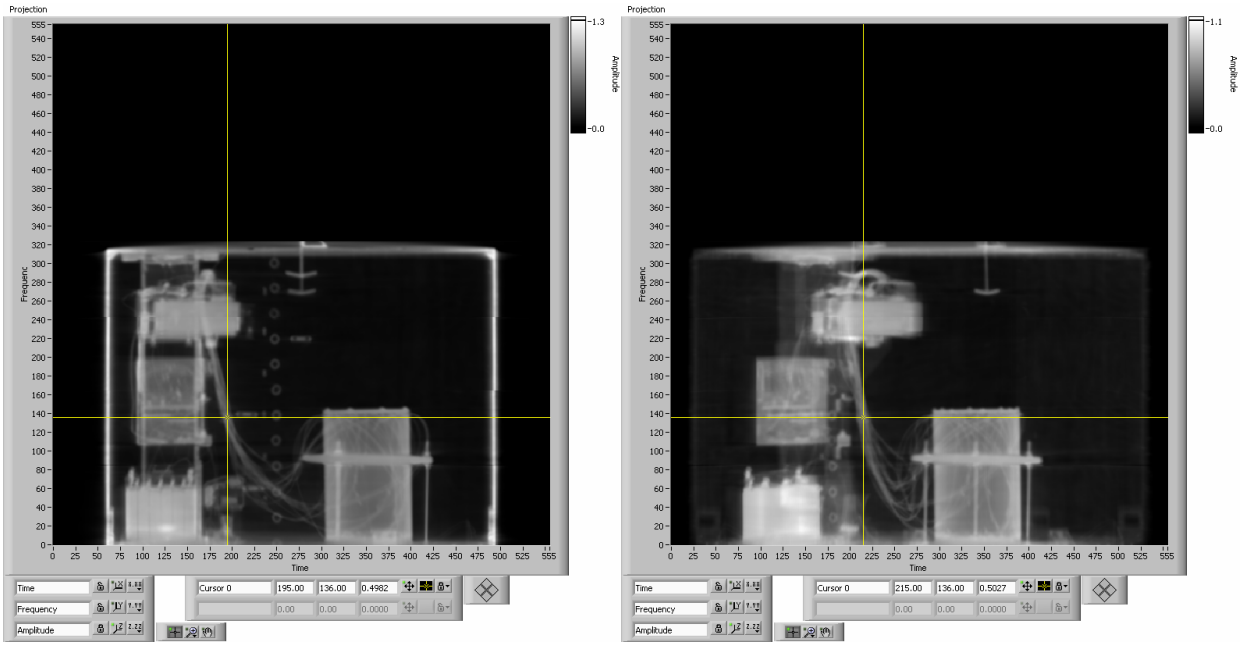

Figure 23: Stereo pair with cursors aligned on wire bundle: 0 degree object rotation (left) and -30 degree object rotation (right).

The coordinates (x_i,y_i) of the wire bundle from Figure 23 are (195,136) for $\theta = 0°$ and (215,136) for $\theta = 30°$. Immediately, we have the y coordinate as 136 from both images above. Proceeding as before, we find:

$$x_1\text{''} = 195 - 278 = -83 \text{ for } \theta = 0°$$
$$x_2\text{''} = 215 - 278 = -63 \text{ for } \theta = 30°.$$

$$-83 = x' \cos(0) + z' \sin(0)$$
$$-63 = x' \cos(30) + z' \sin(30)$$

$$-83 = x' (1.000) + z' (0.0000)$$
$$-63 = x' (0.866) + z' (0.5)$$

$$x' = -83.00$$
$$z' = 17.76$$

$$x = -83.00 + 278 = 195.0$$
$$z = 17.76 + 278 = 295.76$$

The calculated coordinates are thus (195, 136, 295.76) as compared to the actual coordinates of (195, 136, 295) from the CT slice shown in Figure 24. Again, this slight error is probably due to the manual cursor positioning.

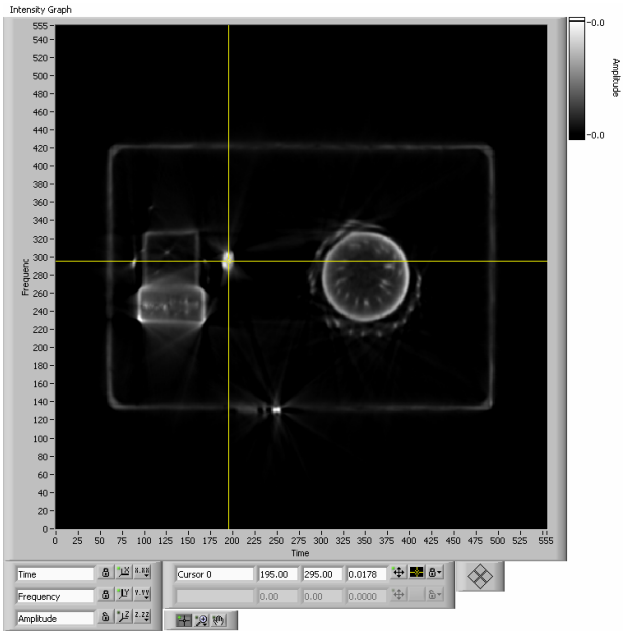

Figure 24: CT slice 136 (rCrate_3057) showing the location of the center of the wire bundle at (195, 295).

Lastly, consider one of the battery terminals as a potential target to disable the device. The coordinates (x_i,y_i) of the battery terminal from Figure 25 are (87,77) for $\theta = 0°$ and (181,77) for $\theta = -45°$. Immediately, we have the y coordinate as 77 from both images in Figure 25. Proceeding as before, we find:

$$x_1\text{''} = 87 - 278 = -191 \text{ for } \theta = 0°$$
$$x_2\text{''} = 181 - 278 = -97 \text{ for } \theta = -45°.$$

$$-191 = x' \cos(0) + z' \sin(0)$$
$$-97 = x' \cos(-45) + z' \sin(-45)$$

$$-191 = x' (1.000) + z' (0.0000)$$
$$-97 = x' (0.707) + z' (-0.707)$$

$$x' = -191$$
$$z' = -53.8$$

$$x = -191 + 278 = 87.0$$
$$z = -53.8 + 278 = 224.0$$

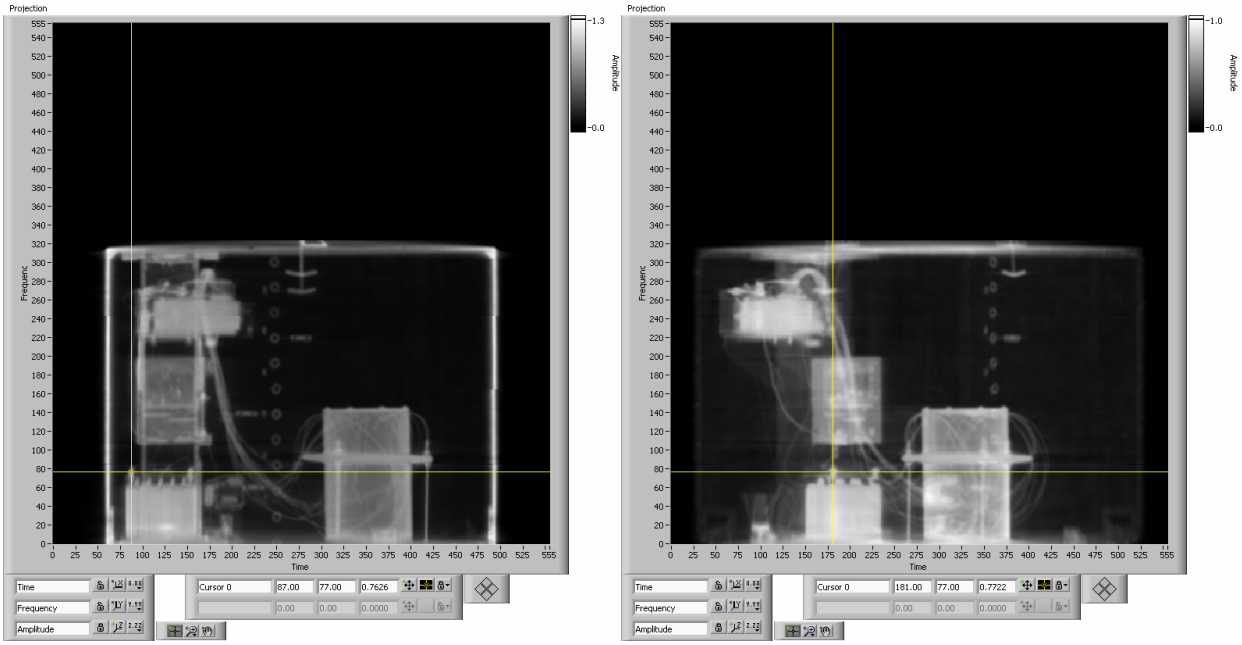

Figure 25: Stereo pair with cursors aligned on battery terminal: 0 degree object rotation (left) and 45 degree object rotation (right).

The calculated coordinates are thus (87, 77, 224) as compared to the actual coordinates of (87, 77, 224) from the CT slice shown in Figure 26.

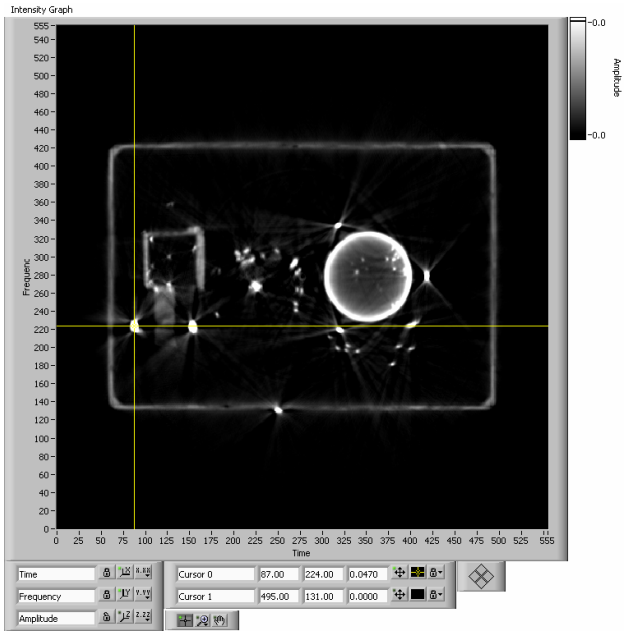

Figure 26: CT slice 77 (rCrate_4036) showing the location of the center of the battery terminal at (87, 224).

Based on the examples provided above, we have demonstrated that a two-view approach for obtaining targeting coordinate information is effective. We used selected CT projections view

angles to calculate the coordinates and compared the results to the CT determined coordinates with excellent agreement.

This method can also be performed with a translation of the source instead of object rotation. This is especially important for field application where the rotation stage equipment may not be available and more importantly the object can not be moved. Thus, the translation method would be the preferred method for use in the field. Both the rotation and translation methods produce a shift in position of a target, or disparity, on the image plane, which is then used to calculate the target position. In the next section of the report, we demonstrate the translation technique with images obtained using the high resolution PSL plates used previously to produce the tiled images of the crate.

Stereo-radiographic Targeting with Source Translation

The team at SRNL believes that the most practical approach to the problem of obtaining target coordinates within an IND involves the use of PSL plates or a thin amorphous silicon flat panel array and a stereo-radiographic targeting methodology. Consequently, we provide in this section an example of this technique using source translation as an alternative to object rotation. The basic approach is depicted in Figure 27. The shift in the projected image point produced by translating the source along the x-axis provides the depth information lacking in a single x-ray radiograph.

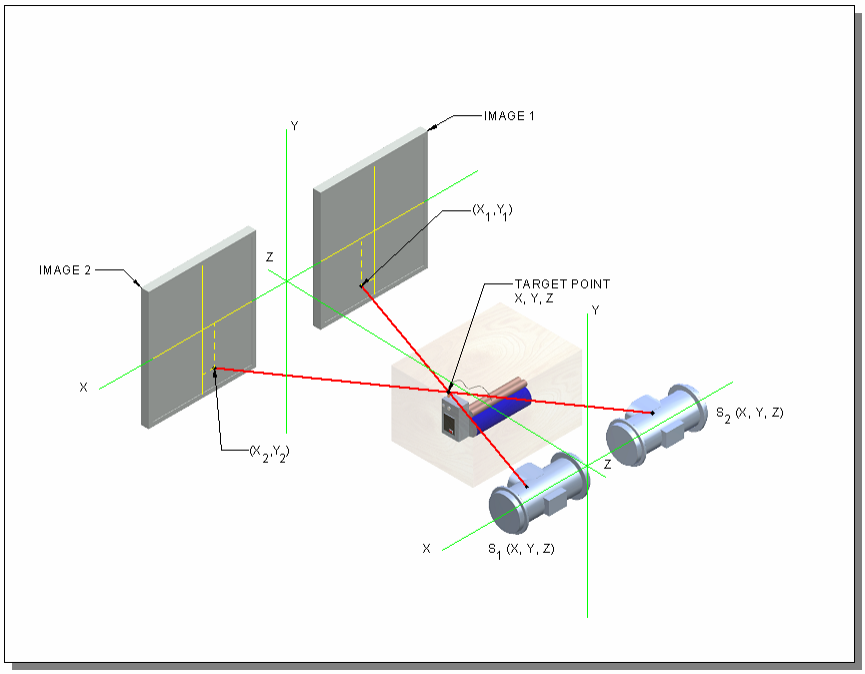

Figure 27: Basic imaging geometry for stereo targeting with source translation.

In the present case, the detectors (PSL plates) were placed in direct contact with the object. In addition, three fiducial markers were placed on the back side of the crate. These markers, which are shown in Figure 28 circled in yellow, allow alignment of the two images. Since these markers are at the back side of the object and on the image plane they have essentially zero disparity. The two images are shown overlapped in Figure 29 with the back plane fiducials aligned and the cursors are aligned on the target point. Figure 29 shows two cursors aligned on the same target point in both images. The distance between the cursors is the target disparity. The object highlighted in red in Figure 29 is on the detector plane and is of known dimensions and will be used for pixel calibration. Lastly, markers (an array of 4 washers enclosed by the green square in Figure 28) were placed on the front of the crate. The shift in these markers provides the maximum disparity, which shall be denoted as δ_{max} , present in the overlapped image. It should be noted that to keep the front fiducial array in both images, it was translated along the x-axis 6 1/8 inches to the left. Any object inside the crate will have a disparity, denoted by δ, between zero and the maximum disparity. In addition, the spacing of front surface

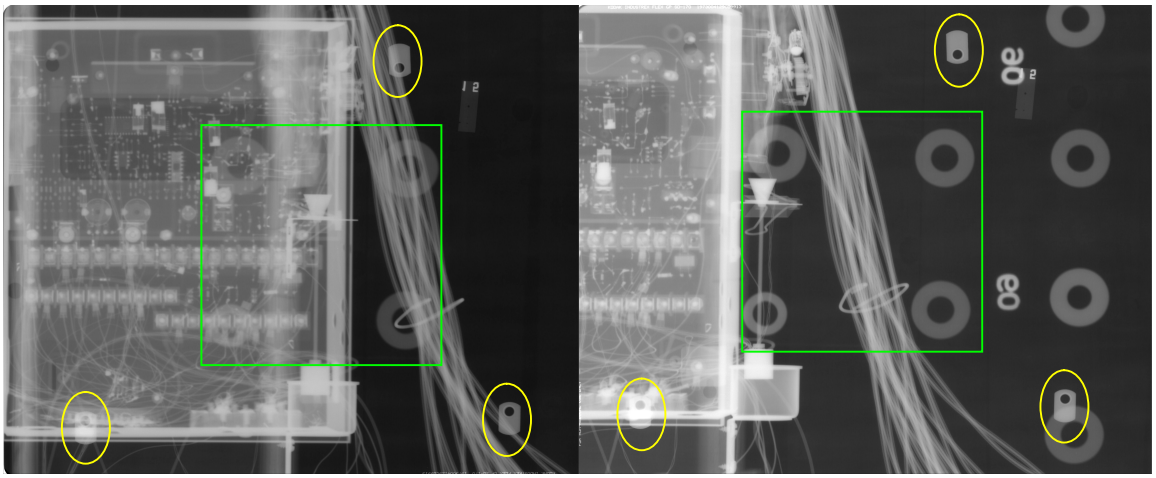

Figure 28: Stereo image pair obtained by translating source 24 inches to the left. Note the disparity between images.

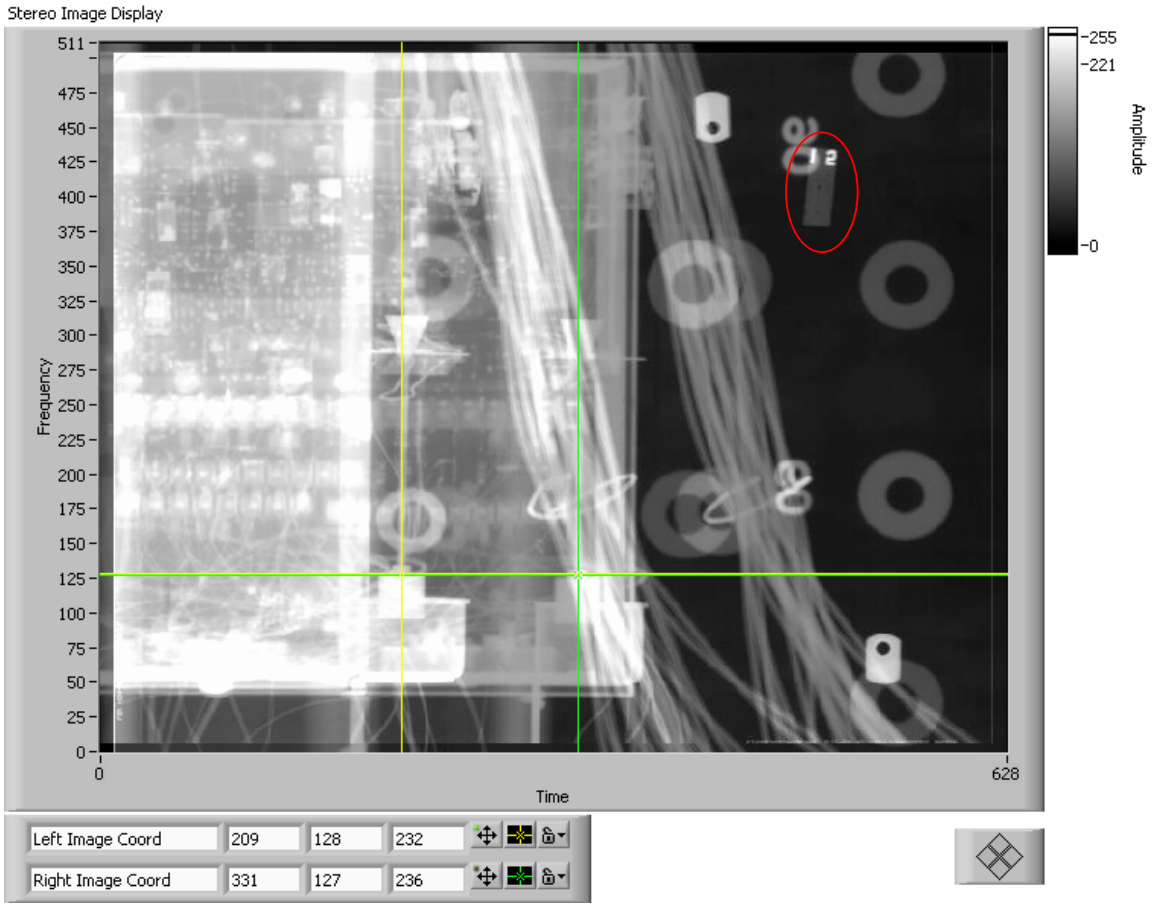

Figure 29: Overlapped stereo-pair created by aligning the detector plane fiducial marks. Both cursors are aligned on the target point.

fiducial marker array can be used to determine the magnification ratio, which is then related to source to detector distance.

The selected target point is better identified for clarity in Figure 30. The selected target is the top of the cylindrical object where the small diameter rod is connected.

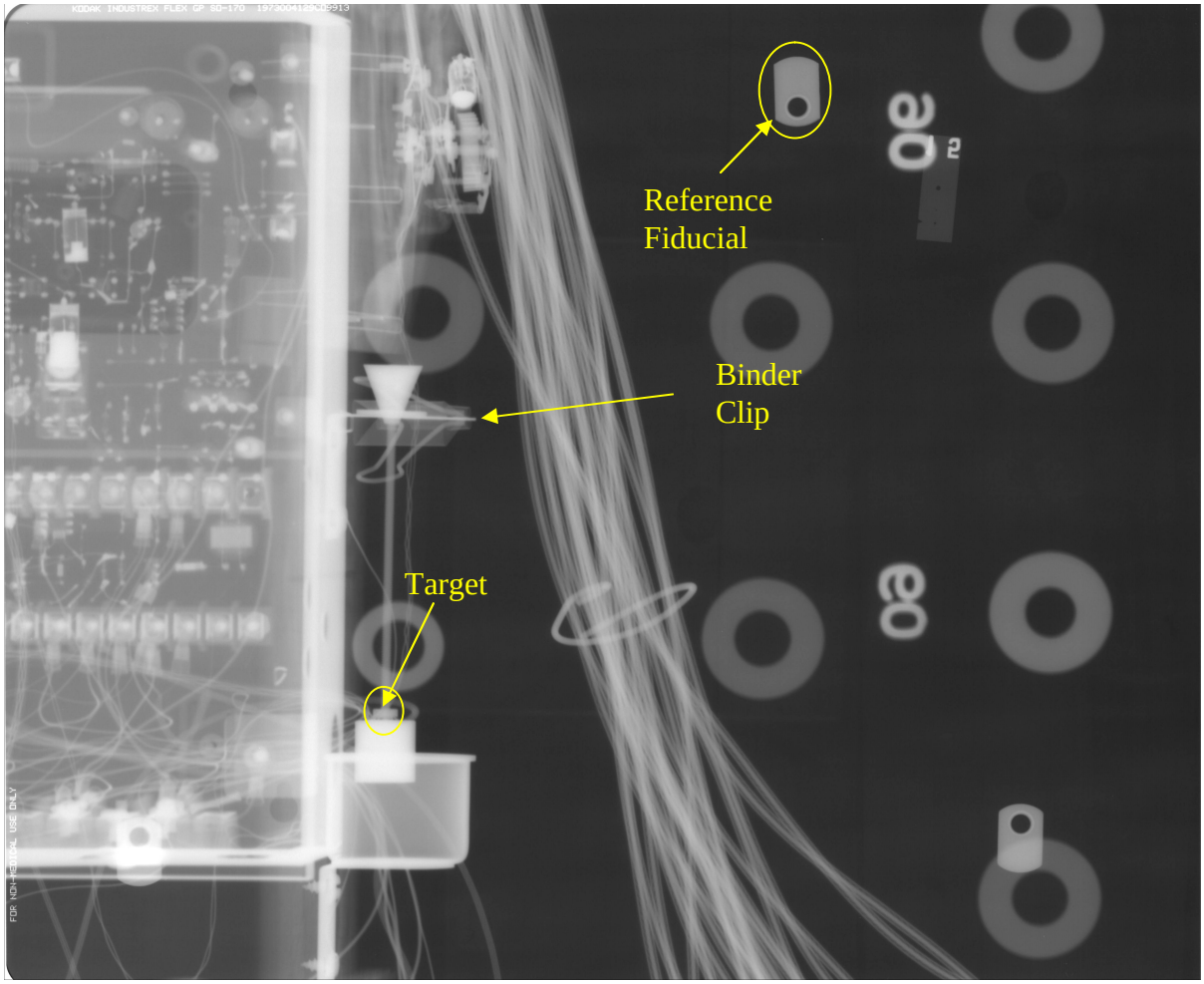

Figure 30: Target location identified in the right image of the stereo pair.

We will now walk through the method for locating this target point from the two images. The depth (z) of an internal target as measured from the detector plane is given by:

$$z = \frac{z_s \mathrm{d}}{(\mathrm{d} - \Delta x_s)}$$

$$\mathrm{d} = x'_2 - x'_1$$

$$\Delta x_s = x_{s,2} - x_{s,1}\,.$$

The disparity, δ, is just the difference between x'_2 and x'_1, which are the image coordinates of the target in the combined stereo image with the detector plane fiducials aligned. In addition, z_s is the source-to-detector distance, and Δx_s is the translation of the source between views. The x-ray source-to-detector plane distance, z_s, was approximately 120 inches and the source translation was approximately 24 inches.

For information, the minimum source translation, Δx_s, required for a desired depth resolution, Δz, and a given target resolution, Δx_{pix}, is given by:

$$\Delta x_s = \frac{\Delta x_{pix}\ z_s}{M_z^2\ \Delta z}$$

Thus, by measuring the disparity of target points in the overlapped stereo-pair the z coordinate is easily found. The x and y values can then be obtained using the following equations:

$$x = x_{s,1} + \frac{(x'_1 - x_{s,1})}{M_z}$$

$$y = y_{s,1} + \frac{(y'_1 - y_{s,1})}{M_z}$$

$$M_z = \frac{z_s}{z_s - z}$$

where $(x_{s,1}, y_{s,1})$ and $(x_{s,2}, y_{s,2})$ are the coordinates of the two source locations and M_z is the magnification ratio at plane z.

The pixel calibration is shown in Figure 31. The distance between the two markers indicated was 3.541 inches. The image is magnified by a factor of 1.364 since it is on the side of the crate closest to the source. The x cursor locations are 250 and 433 for the two cursors shown. Thus, the pixel size is found to be:

$$\Delta x_{pix} = \frac{(3.541)(1.364)}{(433 - 250)} = 0.0264\ \textit{inches}.$$

In addition, the origin of the object coordinate system is defined to be at the back-left-bottom corner of the crate when viewed from the source. Since the origin is not visible in the images, the absolute coordinates of the reference fiducial mark are needed. These coordinates values (x,y) were (15.700, 22.185). These coordinates were measured directly from the bottom-back-left corner of the crate. The pixel size and absolute coordinates of the reference are recorded in Table 3.

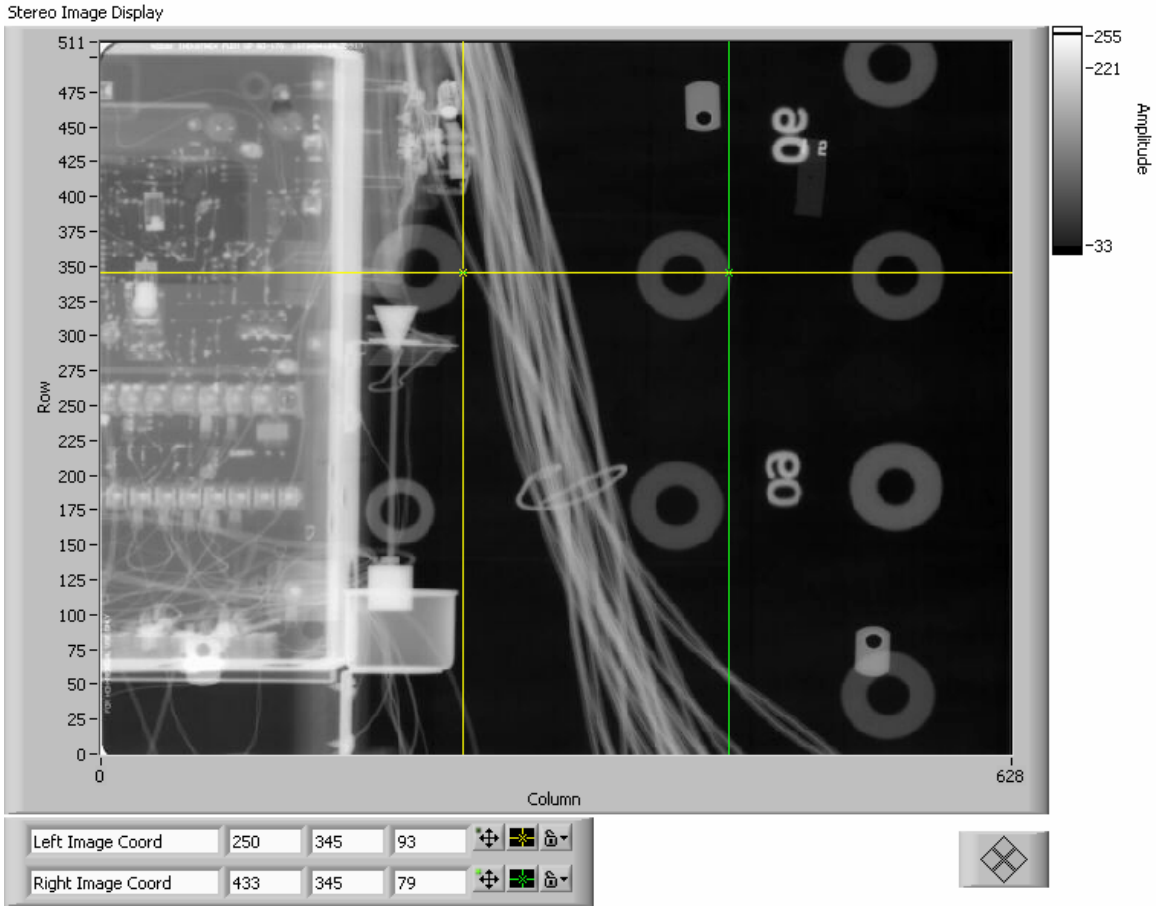

Figure 31: Pixel calibration using the fiducial array.

Table 3: Image pixel size and reference fiducial absolute coordinates.

Pixel Size	0.0264	**in/pix**
Fiducial Abs. Coord		
x	15.700	**inch**
y	22.185	**inch**

Next, the location of the reference fiducial mark and the target point in both the left and right images were measured relative to the left edge of the image for the x coordinate, and relative to the bottom of the image for the y coordinate. These values are recorded in Table 4 as the relative coordinates. The coordinates for the target point are taken from Figure 29 and the coordinates for the reference fiducial are taken from Figure 32.

The coordinates as measured from the fiducial mark are recorded in the columns listed as corrected coordinates. The absolute coordinates (in inches) are found by multiplying the corrected coordinates (indices) by the pixel size then adding the absolute coordinates of the fiducial mark. It should be noted that the absolute coordinates for the left and right image, which are highlighted in yellow, in Table 4 are the projected coordinates of an internal point on the image plane.

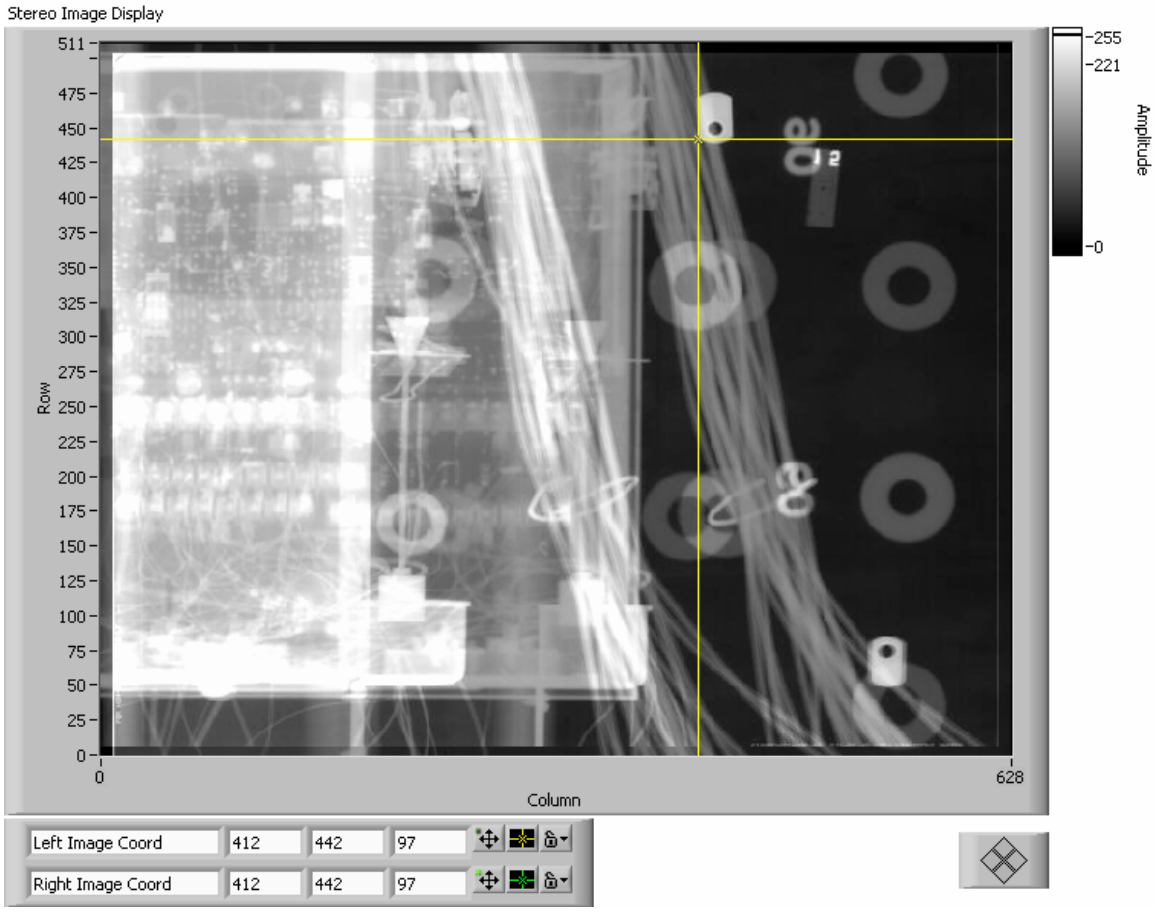

Figure 32: Image showing coordinates of the reference fiducial markers.

Table 4: Fiducial and target coordinates for PSL stereo images.

Left Image				Right Image			
	Relative Coord.	Corr. Coord.	Abs. Coord		Relative Coord.	Corr. Coord.	Abs. Coord
Fiducial	index	index	inch	Fiducial	index	index	inch
x_2'	412	0	15.700	x_1'	412	0	15.700
y_2'	442	0	22.188	y_1'	442	0	22.188
Target				Target			
x_2'	331	-81	13.562	x_1'	209	-203	10.341
y_2'	127	-315	13.872	y_1'	128	-314	13.898

These projected coordinates are transformed into the coordinates of the target point using the equations above. First, the target disparity is calculated:

$$d = x'_2 - x'_1 = 13.562 - 10.341 = 3.221$$

which in turn yields a z coordinate of:

$$z = \frac{z_s d}{(d - \Delta x_s)} = \frac{(120)(3.221)}{3.221 - (-24)} = 14.199 .$$

Using the calculated z coordinate and z_s, the magnification factor is calculated as:

$$M_z = \frac{z_s}{z_s - z} = \frac{120}{120 - 14.199} = 1.134 .$$

We now find the x and y coordinates using the magnification factor and the equations above. We also need one of the source locations. In position 1, the source was located at the coordinates (24, 18, 120) with respect to the crate coordinate system. Thus,

$$x = x_{s,1} + \frac{(x'_1 - x_{s,1})}{M_z} = 24 + \frac{(10.341 - 24)}{1.134} = 11.955$$

$$y = y_{s,1} + \frac{(y'_1 - y_{s,1})}{M_z} = 18 + \frac{(13.872 - 18)}{1.134} = 14.360$$

It is now desired to find the actual coordinates of this target point so that the error can be determined. As earlier, we use the CT data set to find the "actual" coordinates at least within the resolution of the CT data set (~0.1094 inch).

The CT slice in Figure 33 can be used to find the x and z coordinates with respect to back corner of the crate. The x and z coordinates are calculated as follows:

x = (168 – 58)(0.1094) = 12.03 inches
z = (425 – 295)(0.1094) = 14.22 inches

The y coordinate can be determined from the parallel ray projection through the CT data set at a view angle of 0 degrees, which is shown in Figure 34. The y coordinate is thus:

y = 36 inches - (318 – 122)(0.1094) = 14.55 inches

Note that we subtract the distance obtained from Figure 34 from the height of the crate (36 inches), so that the y coordinate will be measured from the bottom of the crate.

The target coordinates calculated using the two-view stereo-radiography approach and the actual target coordinates obtain from CT are summarized in Table 5. In addition, the absolute errors are shown. These results are excellent since the absolute errors are on the order of the CT resolution element (0.1094 inches) and less. It is likely that if the CT resolution had been better the calculated errors may have been smaller.

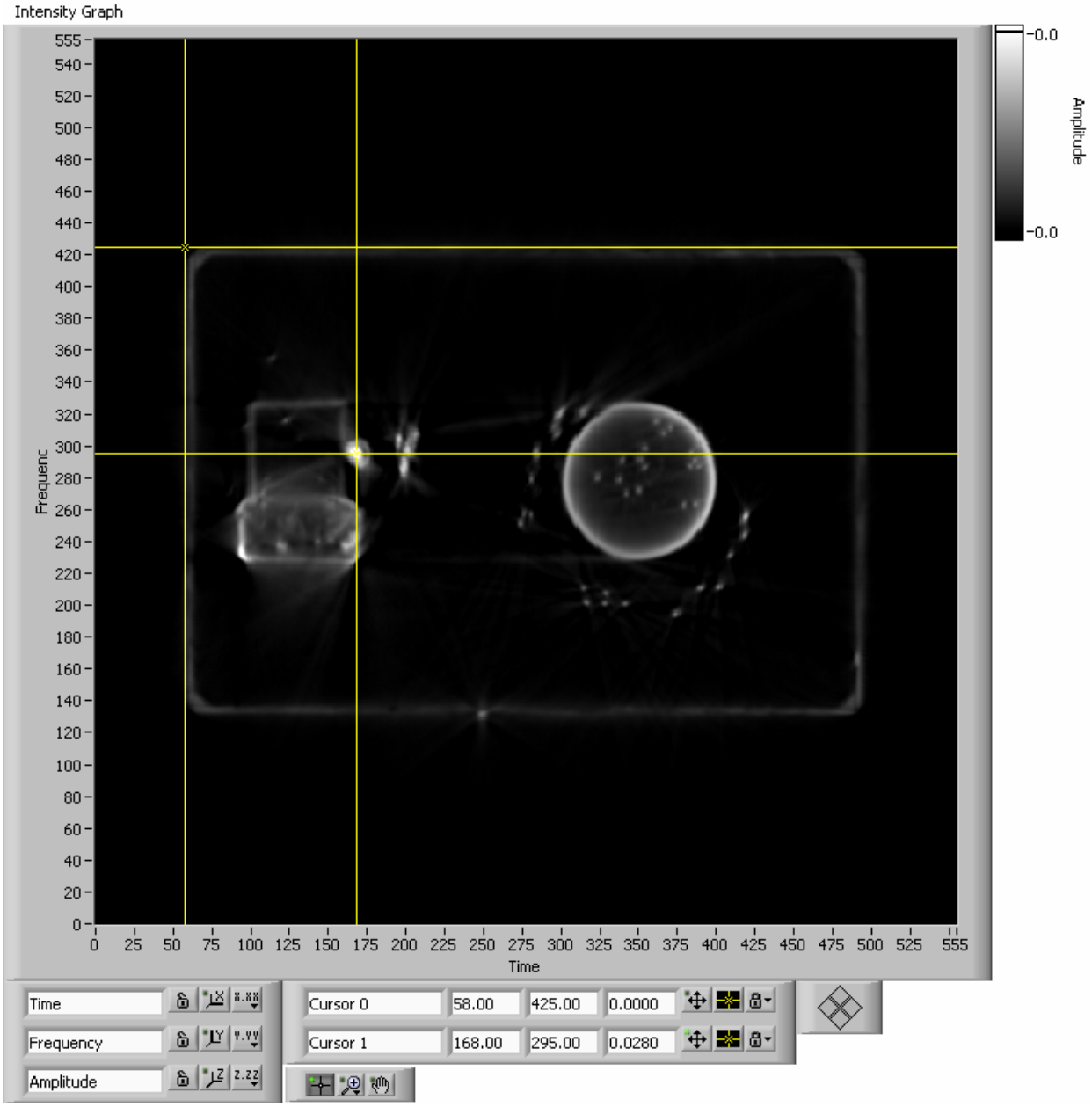

Figure 33: CT slice (rCrate_3075.sdt) showing location of the target point and corner of crate.

The y coordinate has the largest error because we had to use the crate height (36 inches) in the calculation of the actual coordinate from the CT projection, since the bottom of the crate was not visible in the projection. The 36-inch value is a nominal height and it probably varied +/- 0.125 to 0.250 inches around the crate.

Nonetheless, we have demonstrated that this technique has the potential to provide accurate targeting information without the need to perform CT. This method is less cumbersome than CT to perform in a field environment. The SRNL team believes this technology is worth pursuing in future work to provide first responders with the means to rapidly obtain the information necessary to disrupt an IND.

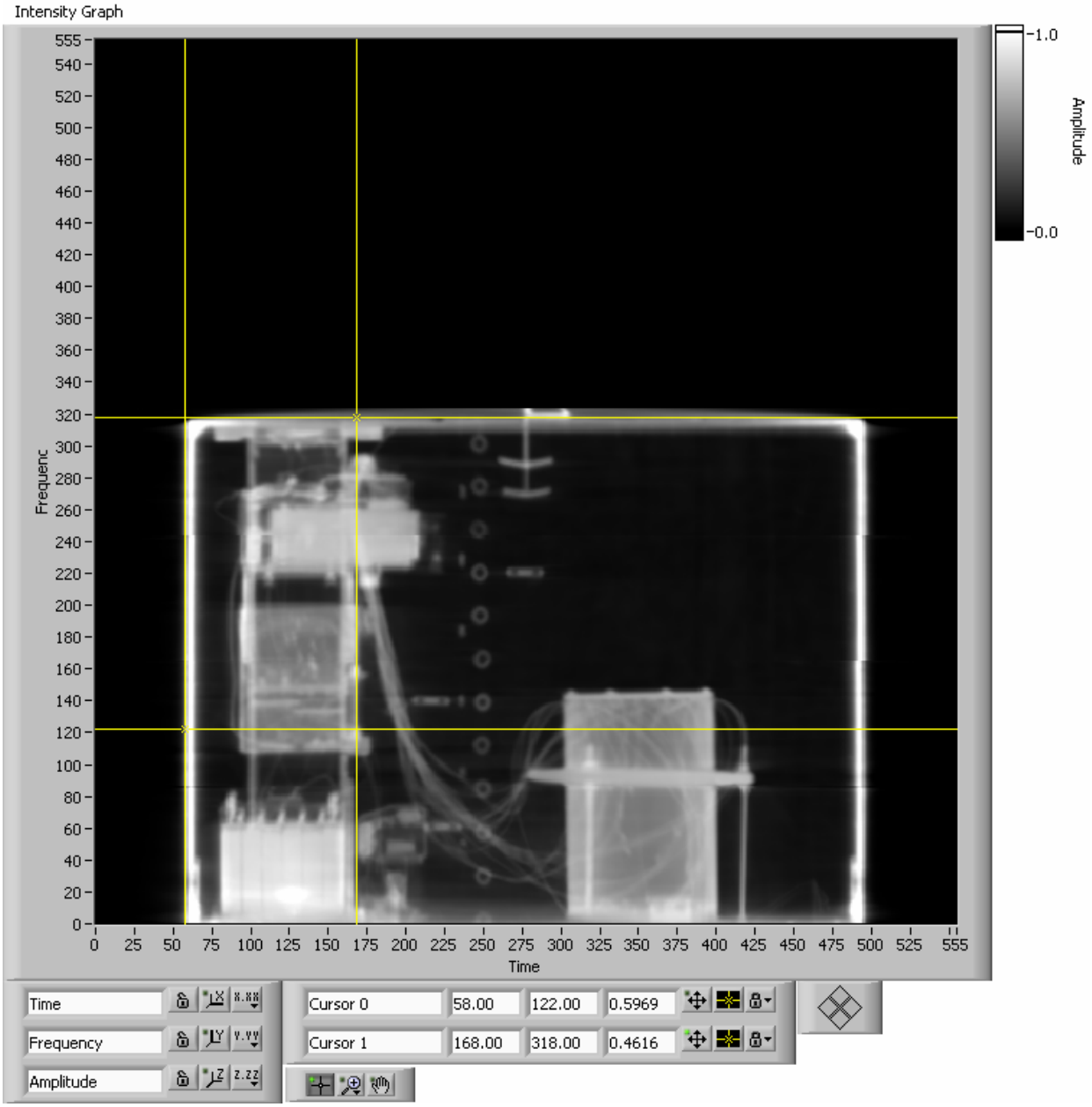

Figure 34: Parallel ray projection through CT data set at a view angle of 0 degrees, which provides the x and y coordinate of the target point.

Table 5: Summary of calculated target coordinates and error.

Target Coord.	Calc. (inch)	Actual (inch)l	Abs. Error (inch)
x	11.955	12.030	0.075
y	14.360	14.550	0.190
z	14.199	14.220	0.021

Application of Stereographic Vision Hardware

In addition to precise targeting, two images of an object obtained by object rotation or source translation can be used to produce a 3-D image using the appropriate stereographic hardware. The utility of this approach is that the user gains more insight into the internal geometry of the object without the need to collect a large CT dataset or perform time consuming CT reconstructions. Furthermore, there is no need for mechanically complicated CT imaging equipment. This technique can be done by a simple translation of a portable source.

This qualitative 3-D data provided by this approach can be useful for determining whether an object is in front or behind another object. This information is important in the determination of the best path to the target coordinates, when planning the approach for device disruption.

The SRNL team has procured the system shown in Figure 35 and have successfully produced several x-ray stereo-images. Unfortunately, these results can not be presented in a hardcopy report.

Figure 35: Stereographic viewing equipment which includes 120 Hz monitor, polarizing screen, and polarized goggles.

Summary

This report has documented the worked performed in the x-ray computed tomographic and stereo-radiographic inspection of the NA-42 test object. We have described the method SRNL used to obtain high resolution (80 micron) images of the test object using PSL plates. The PSL plates are an excellent alternative to x-ray film and they eliminate the need for the wet chemistry processing and the disposal of the chemical wastes. The PSL plates were used to provide an overall panoramic view of the large test object. These images were useful in planning other inspection techniques.

In addition, a customized digital radiography system with an 85-inch wide field-of-view was assembled to support the data collection for computed tomography. The trade-offs between resolution and data collection and CT reconstruction time were explained in detail. The CT projections and reconstructed slices of the test object were included in the report as static images and "movies" were also provided on the attached CD-ROM. The combination of the projections and the CT slices provide a thorough understanding of the internal structure of the device. The full projection CT results were also used as a "bench mark" for other techniques investigated during this work, such as the limited view CT and stereo-radiographic work.

The limited view CT results were obtained by parsing the full data set into subsets with larger angular intervals and thus fewer projections. These subsets were then processed with the CT reconstruction software. The results of reconstructions from 720 down to 10 projections were compared. Based on these results, we concluded that 20 to 30 projections were adequate. These results were then used to predict the required data collection time for higher resolution systems. It was concluded that from a data collection time basis, limited view CT could provide the desired resolution (1 mm) within a reasonable period of time. However, there were other considerations related to actual field conditions that might preclude the use of CT. Consequently, SRNL also investigated other techniques.

If the objective of the inspection is to provide the coordinates of key components of an IND, then CT is not needed. SRNL has shown that stereo-radiography using relative object-imaging system rotation or source translation are both effective in providing accurate targeting information. A detailed explanation, including examples, of these techniques was provided in this report. SRNL also believes that the accuracy of the techniques can be dramatically improved in future work, because several key parameters were measured using a tape measure. For example, a 3-D fiducial array could be used to determine key parameters without a need for direct measurement. A higher degree of accuracy in the determination of those parameters will enhance the accuracy of the overall technique. In addition, since the actual internal geometry of the test object was unknown, the CT results were used to validate the other methods. However, the calculated error in the target coordinates were on the order of the resolution of the CT results (0.109 inches). A better test of the techniques would be to construct a test object where the target points are measured with a higher degree of accuracy than the technique to be proven.

A brief discussion on the usefulness of stereo-graphic vision equipment was also included. The main benefit of this method is to provide field personnel with qualitative "3-D" information without the need to collect a CT dataset or perform a tomographic reconstruction.

Based on these results, SRNL recommends that the best approach at determining target locations is to utilize the stereo-radiography approach using source translations and fiducial markers. Lastly, the PSL plates or ASi flat panel imagers offer the most practical detector choice for a field application.